uc3m | Universidad Carlos III de Madrid

University Degree in Aerospace Engineering

Academic Year 2018-2019

Bachelor Thesis

GENERATION OF GRAVITY WAVES IN AN EXPERIMENTAL FACILITY

Author: Andrea de la Sen Osende

Tutor: Javier Rodríguez Rodríguez

Madrid, June 2019

ABSTRACT

The development of a computational tool to study the propagation of gravity waves in water is carried out by reproducing the conditions of an experimental study. The problem consists in the propagation of a gravity wave in a channel with a bottom topography where the is already a mean flow in the opposite direction. The physics of such problem is analogous to the one involved in the Hawking radiation of a black hole, which stresses the practical importance of the computational tool being developed, given that black holes are phenomena difficult for us to study.

The problem will be analyzed with both a theoretical and a numerical approach. The numerical simulations will be performed by means of the software *Gerris*.

As a first approach, a simpler version of the problem in which the channel is straight is analyzed. From the theoretical point of view, in these conditions and under some assumptions about the nature of the flow, the equations describing the motion of the fluid (Navier-Stokes equations) can be simplified up to a linear theory which provides an analytical solution. The analytical linear results are then contrasted with those obtained with a numerical simulation in order to check the validity of the latter. Once this step is accomplished, the actual problem of a flow in channel with a bottom topography will be studied by means of a numerical simulation, using the same computational methodology. The results obtained will be compared to those obtained in the experimental study mentioned earlier. The aim of this project is to implement a numerical tool that allows us to investigate up to which point the experimental analogy between gravity waves propagating against a flume in a channel of variable depth and the Hawking radiation of a black hole is applicable. The computational tool we will derive can be later extended to the study of the propagation of water gravity waves in flows under different conditions.

Keywords: Water gravity wave, dispersion relation, Froude number, topography, numerical simulation, computational tool, *Gerris*.

To Javi, for teaching me the beauty of science,

and for being there all the way to here.

CONTENTS

LIST OF FIGURES

1. GENERAL INTRODUCTION

1.1. Motivation

The idea for this project came as a result of the study performed by Silke Weinfurtner et al. published in the article *Measurement of Stimulated Hawking Emission in an Analogue System* in the *Physical Review Letters* [1]. In such article, the authors aim to understand the behaviour of the so-called Hawking radiation of a white hole (time-reverse of a black hole) by establishing an analogy with the propagation of surface gravity waves in water.

In Physics, a surface wave is a wave (a perturbation) perpendicular to the interface between two media, that propagates along this interface. The propagation of the wave along the interface is due to the action of some restoring force that tries to bring the system back to its initial position. In the case in which this force is gravity, the resulting waves are called gravity waves.

In the article mentioned above, the authors show by means of experimental data that when a long wave (shallow-water wave) that is propagating in water channel due to the action of gravity, reaches a region of high flow velocity opposing its motion, it is blocked and later on decomposed into two shorter waves (deep-water waves) that propagate in the opposite direction to the one of the initial wave. The physics of such problem is analogous to the one governing the Hawking radiation of a black hole. Therefore, the interest of such study lies in the fact that it enables to take an experimental approach on a problem that is otherwise unattainable.

In this project, we aim to implement a numerical tool with which we can reproduce the results obtained in such experiment by means of a numerical simulation. However, note that the analysis performed to get to this point and the tool that will be finally developed are not restricted to the particular experimental case with which the procedure will be illustrated. In contrast, this tool may be used in any study concerning the propagation of gravity waves in water or any other fluid. In particular, regarding the aerospace industry, gravity waves are a relevant phenomena to take into consideration and several applications can be found in which the computational methodology that will be developed may result

useful. To list some of them:

- Seaplanes.
- Ditching and splashdown.
- Interaction of aircraft carriers with waves.
- Sea platforms for take-off and landing of aircraft and spacecraft.
- Sloshing in aircraft fuel tanks or spacecraft tanks in the early stages of the launch.

a) 

b) 

c) 

d) 

Fig. 1.1. Examples: a) Seaplane [2], b) Apollo 16 splashdown [3], c) Aircraft carrier [4], d) SpaceX Falcon 9 first stage after landing [5]

Computational tools are continuously gaining strength in both scientific and engineering applications due to their potential use to predict with accuracy the response of a system under some conditions, and to help in the understanding of some physical phenomena without the need of conducting excessive experiments. The great utility use of

such tools is obvious in both fields, and this is why the methodology we present in this project is of practical importance.

1.2. State of the art and literature

The problem of the propagation of gravity waves in water is a complex problem, mainly due to the non-linearities governing the flow equations and to the possible random nature of the waves. Even if the oscillations happen to be periodic, the interaction between waves and a current and wave-blocking are phenomena not yet deeply understood. The propagation of gravity waves in water is a very wide field of study and as such, research and experiments conducted can be found in the literature ranging from Quantum Mechanics studies to Coastal Engineering and Oceanographic projects.

Regarding Quantum Mechanics applications, as mentioned above, a big part of the research being conducted nowadays concerns the experimental analogy between the Hawking radiation of a black hole and the blocking of surface water waves in a channel with a mean current and a varying depth. Several recent studies can be found in the literature ([1], [6], [7]), but the experiments are not yet entirely conclusive and further research in the field is needed.

On the other hand, the interaction of structures with waves is an important issue in coastal projects and maritime facilities such as harbors, docks or sea platforms. The design of such structures is a common topic in the literature and several books and studies can be found ([8], [9]). Moreover, an emerging field of study in relation to engineering is that of the sloshing of fuel inside tanks of aircraft, spacecraft and carrier ships. Such phenomena may compromise the stability of the whole structure and it is currently a challenge for the industry. Most of the studies conducted involve CFD simulations ([10], [11]).

1.3. Structure and procedure

In order to perform a complete study, concepts of Physics, Fluid Mechanics and Numerical Methods are needed. First of all, given the importance of the physical background in the problem, some notions on the physics of waves are provided. The next step will

consist in studying a simpler version of the problem in order to develop the theoretical notions and the numerical tools that will be used later on to analyze the actual case that concerns us. Starting from the Navier-Stokes equations, which describe the motion of a fluid, we will apply some simplifications so as to arrive to the so-called *Airy Wave Theory*. Such theory provides the linear solution of the Navier-Stokes equations for the flow of and ideal fluid in a constant-mean-depth domain. A numerical simulation will be then carried out for a flow and a domain with the same characteristics. The results will be compared and discussed. Once the numerical methodology has been proven to work successfully, the simulation domain will be modified to coincide with the one used in the experiments performed by S. Weinfurtner et al. The results obtained will be commented as well. All in all, this report will be structured as follows:

- **Chapter 1 - The physics of waves:** a solid physical background on the nature of waves is needed in order to properly understand the problem. What a wave is, how it is created and its main characteristics are defined in this section.

- **Chapter 2 - Theoretical analysis:** the theoretical analysis starts with the formulation of a simpler version of the actual problem: the interaction of a current flowing in a straight channel with incoming waves. The assumptions that will bring us to Airy Wave Theory are introduced and justified. Under these assumptions, the equations describing the motion of the fluid (Navier-Stokes' equations) are simplified up to Laplace's equation (Potential Flow Theory). The boundary conditions of the problem are also defined and linearized. The problem is then solved by means of two different approaches, both of which lead to the same important equation: the dispersion relation. Fourier Analysis is introduced as the tool to study the evolution of a wave in time. Finally, the bottom topography is introduced and a new theory (Shallow Water Theory) will be needed in order to study the evolution of the flow in a channel of variable depth.

- **Chapter 3 - Numerical simulation:** the open-source software used in order to performed the numerical simulations, *Gerris*, is presented and its main features are described. The numerical set-up for both the straight channel domain and the channel with a bottom topography are explained in detail.

- **Chapter 4 - Results:** the theoretical and numerical results obtained for the linear problem are compared and discussed. The limits of the linear theory are also briefly commented. Finally, the results obtained for the simulation of an initial perturbation reaching the throat of the channel, where the flow is at critical conditions, are presented and analyzed.

- **Chapter 5 - Conclusions and future work:** the main points to be extracted from the project are outlined. Possible improvements and points to delve into in further studies are considered.

1.4. Budget and regulatory framework

Given the theoretical nature of this study, a budget cannot be specified since actual experiments were not performed. The data used relies upon experiments carried out by other authors and upon the numerical simulations that will be described in detail later on. The software for such simulations is open-source, and the programming tools used for post-processing (Python and MATLAB) are either open-source as well, or accessible by means of a student license provided by Carlos III University.

Regarding the regulatory framework, the conclusions extracted from this study can be used for the analysis and design of engineering structures that interact with gravity waves, as mentioned above. Such structures can go from sea platforms (subjected to recommended practices and certification regulations [12], [13]), to aircraft carriers (subjected to the SOLAS convention [14], and the Naval Ship Code issued by the NATO [15]) or fuel tanks (subjected to Fuel Tank Safety recommendations issued by the FAA [16] and the EASA [17]), to give some examples.

2. THE PHYSICS OF WAVES

A wave is the propagation of a perturbation in a medium. A perturbation is a deformation of the medium caused by some external agent. This deformation creates local stresses on the particles that are be transmitted to the neighbouring particles resulting in the propagation of the deformation, i.e, the wave. In particular, water waves "are a manifestation of forces acting on the fluid tending to deform it against the action of gravity and surface tension, which together act to maintain a level fluid surface" [18]. The longer the wave is, the smaller the effect of surface tension on its motion. The particular case for which the effect of surface tension is negligible and the motion of the wave in the fluid is governed by gravity, are the so-called gravity waves, meaning that gravity is the only force which tries to bring the system back to equilibrium. In other words, as Landau and Lifshitz explain, initially, the free surface of a liquid in equilibrium in a gravitational field is a plane. If a perturbation occurs at some point, the surface will move at this point, and then the motion will propagate all over the surface in the form of waves. This type of waves are called gravity waves because their propagation is due to the action of the gravitational field [19]. It is worth mentioning as well that even if gravity waves appear on the surface of the liquid, they have an effect on the interior of the body of liquid that decreases as depth increases. Note also that the free surface aforementioned is the region of the body of liquid that separates it from the atmosphere. This region is subjected to zero tangent shear stress, due to the usually negligible viscosity of air.

2.1. Wave Parameters

In order to be able to characterize the motion of the wave, some parameters need to be defined. Since for the present case the motion of the wave is confined within a channel, the water depth and the length of the channel need to be introduced being referred to as H and L from now on, respectively.

- a: semi-amplitude. This is, the distance from the still free surface ($z = H$) to a wave crest.

- λ: wave length. Distance from crest to crest in the x axis.
- k: wave number, $k = 2\pi/\lambda$. The wave number can be regarded as the spatial frequency of the wave, i.e, the number of cycles the wave completes in the spatial unit.
- T: wave period.
- ω: wave (temporal) frequency, $\omega = 2\pi/T$.
- v_p: phase velocity (also called *Celerity*), $v_p = \lambda/T = \omega/k$. It is the speed at which each frequency component of the wave packet propagates.
- v_g: group velocity. It is the velocity at which the wave envelope (overall shape of the waves' amplitudes) propagates, $v_g = \partial\omega/\partial k$, evaluated at the central frequency.

2.2. Physical properties of waves

Waves exhibit some interesting physical behaviours that are worth mentioning.

- **Reflection:** it consists in the change of direction of the wave when it strikes a reflective surface.
- **Refraction:** it consists in the change of the wave's phase velocity when the it passes from one propagation medium to another.
- **Diffraction:** it is a phenomena by which the wave bends when it meets an obstacle or when it comes out of an opening.
- **Absorption:** absorption takes place when the wave strikes on a surface and its energy is absorbed by the material of the surface.
- **Interference:** interference is a characteristic property of waves by means of which, different waves that meet, create a new wave that results from the superposition of them.
- **Dispersion:** dispersion is a phenomena that appears whenever the phase velocity of the wave depends on its frequency or wavelength. This dependency is expressed by means of the so-called *dispersion relation*.

2.3. Wave types

Waves can be divided into a wide range of classes. In this way, one can find electromagnetic waves, mechanical waves, quantum mechanical waves, gravitational waves, etc. Water waves are a type of mechanical waves (matter oscillates and energy is transferred trough the medium) and they can as well be classified into different groups. One of these classifications attends to the water's relative depth in the channel, H/λ, and it is as follows:

- **Shallow water waves:** $H/\lambda < 0.05$.
- **Intermediate depth waves:** $0.05 < H/\lambda < 0.5$.
- **Deep water waves:** $H/\lambda > 0.5$.

It is important to note that the aforementioned *dispersion relation* changes in each of the situations given above. Also, it is interesting to take a look at the trajectory of the fluid particles in each of these situations (Figure 2.1).

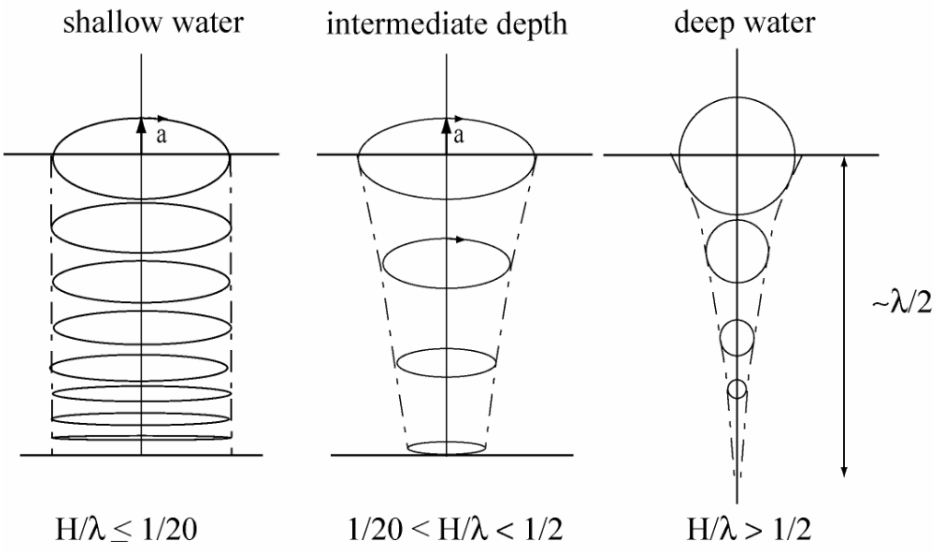

Fig. 2.1. Particles trajectories for different water's relative depths. [20]

As it can be seen, the trajectories of the fluid particles change, describing elliptic orbits of decreasing eccentricity (up to zero for the case of a circular orbit) as the relative depth of water increases. Moreover, the horizontal component of the velocity decreases from the surface to the bottom illustrating the fact that, as the relative depth of water increases,

the fluid particles that are far from the free surface are not affected by the motion of the free surface.

3. THEORETICAL ANALYSIS

Once an introduction into the physics of waves has been given, the case under study will be now analyzed from a theoretical point of view.

3.1. Problem formulation

Let us begin the theoretical analysis by assuming first a straight channel (without a topography at its bottom), as it is a simpler case that will provide the reader with a first insight into the problem and with a base to better understand the actual case under study presented in this report.

In such a case, the problem to be solved is that of determining the behavior of water when it is flowing in a straight channel in a given direction with a given velocity, and it encounters incoming waves in the opposite direction of its motion. See Figure 3.1 for a schematic representation of the problem's geometry.

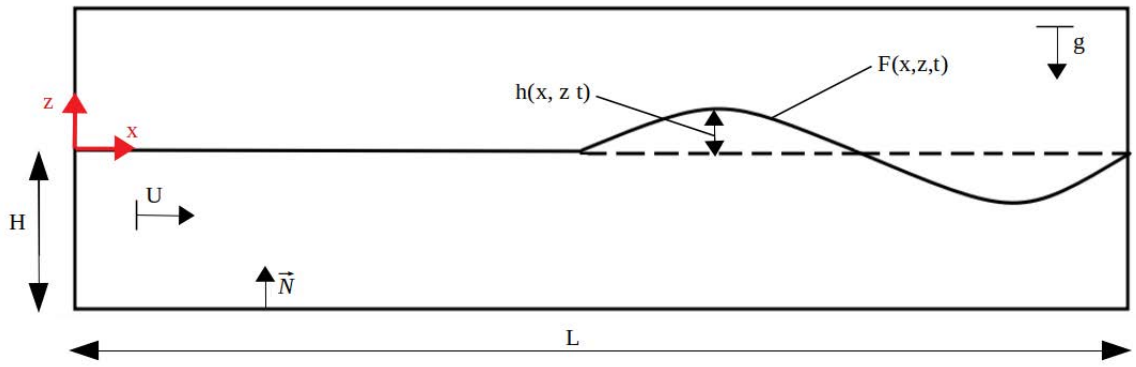

Fig. 3.1. Sketch of the problem's geometry.

Note that the reference frame that will be used in all the subsequent analysis is defined with its origin in the still free surface. The x axis is the horizontal axis, with the positive direction to the right, the z axis is the vertical axis, with the positive direction up, and the y axis is given by the right-hand rule.

The objective of the theoretical analysis is to obtain analytical expressions for the

velocity potential and the wave amplitude that will allow us to obtain the values of these variables at any point of the domain, at any given time. These are chosen as the unknowns of the problem because measurements of them can easily be taken and contrasted with values reported in the literature.

3.2. Assumptions

Before writing the equations that model the motion of the fluid and the boundary conditions of the problem, some assumptions about the nature of the flow can be made in order to simplify the subsequent analysis.

3.2.1. Incompressible flow

In fluid mechanics, the compressibility of a fluid quantifies the change in the volume of the fluid when a change in its pressure takes place. The compressibility of a fluid (β) can be expressed in terms of its bulk modulus, here denoted by B and defined as $B = \rho \partial p / \partial \rho$, as in Equation 3.1.

$$\beta = \frac{1}{B} = \frac{1}{\rho} \frac{d\rho}{dp} \tag{3.1}$$

The bulk modulus for water is $B = 2.15 \cdot 10^9$ Pa, therefore, its compressibility is of the order of 10^{-9} and can be considered negligible. This means that the density of a fluid particle of water remains constant all along its motion. Equation 3.1 can be rewritten for the case of water as:

$$\frac{1}{\rho} \frac{d\rho}{dt} = \frac{1}{B} \frac{dp}{dt} \approx 0 \tag{3.2}$$

Introducing now the Navier-Stokes Continuity Equation,

$$\frac{\partial \rho}{\partial t} + \rho \nabla \cdot \vec{v} + \vec{v} \cdot \vec{\nabla} \rho = 0 \tag{3.3}$$

where $\vec{v} = (dx/dt, dy/dt, dz/dt)$ and, therefore, $\partial \rho / \partial t = d\rho / dt \approx 0$ (from 3.2). One may see that the fact that the fluid is incompressible necessarily implies that it is *nondivergent*

or *solenoidal*, i.e, that the divergence of the velocity is zero in all the domain:

$$\vec{\nabla} \cdot \vec{v} = 0 \tag{3.4}$$

3.2.2. Inviscid flow

The Reynolds number of a flow is defined as:

$$Re = \frac{\rho U L_c}{\mu} \tag{3.5}$$

where U is the flow velocity and L_c is the characteristic length of the problem, in this case the water height of the still free surface. When the Reynolds number of a flow is very large, it can be approximated to an inviscid flow, i.e, one with zero viscosity. For this particular case, the density and the dynamic viscosity of water at 25 °C are 997 kg/m^3 and $8.91 \cdot 10^{-4}$ kg/(m s), respectively. The water height of the still free surface is of the order of 10^{-1} meters, and the velocity of the flow will be of the order of 1 m/s. These values have been chosen based on experiments already performed and that can be found in the literature ([21], [22], [1]). Under these considerations, the Reynolds number of the problem will be of the order of $O(Re) \sim 10^6$, which is sufficiently large to consider the effect of viscosity negligible in the fluid's motion.

3.2.3. Irrotational flow

The vorticity of a flow is a vector field defined as the curl of the flow velocity:

$$\vec{\zeta} = \vec{\nabla} \times \vec{v} \tag{3.6}$$

For an irrotational flow, the curl of the velocity field is zero and, therefore, the vorticity is zero. According to *Kelvin's circulation theorem*, an inviscid flow that is irrotational at some instant in time, will remain irrotational. Given that the flow of the problem at hand has an initial velocity field that is irrotational (because the water is flowing with a uniform horizontal velocity component in the channel) and because the flow is inviscid, the flow can be considered irrotational at all times.

3.2.4. Potential flow

A potential flow is one in which the velocity field can be derived as the gradient of a scalar function called the *velocity potential*, ϕ. Given that the flow is irrotational, $\vec{\nabla} \times \vec{v} = 0$, we can define the flow velocity as the gradient of some scalar function, $\vec{v} = \nabla\phi$, since the curl of a gradient is always zero. The motion of a potential flow can be studied by means of the *Potential Theory*, which consists in the study of harmonic functions. This step simplifies greatly the analysis.

3.2.5. No surface tension

The Bond number is used to characterize the importance of gravitational forces against surface tension in the interface between two fluids. It is defined as:

$$Bo = \frac{\Delta\rho g L_c^2}{\gamma} \tag{3.7}$$

where $\Delta\rho$ is the difference in density of the two fluids and γ is the surface tension. In this case, $O(\Delta\rho) \sim 10^3$, $O(L_c) \sim 10^{-1}$, $O(g) \sim 10$ and $O(\gamma) \sim 10^{-2}$. Therefore, the order of magnitude of the Bond number is $O(Bo) \sim 10^4$, which is large enough to consider the surface tension negligible.

3.3. Governing equations and boundary conditions

Under the assumptions given in the previous section, the motion of the flow can be modeled by means of Potential Theory. This means that the velocity potential will satisfy Laplace's equation:

$$\nabla^2\phi = 0 \tag{3.8}$$

Which is obtained by introducing the flow velocity expressed as the gradient of the velocity potential into the non-compressibility condition, Equation 3.4.

In order to find the expressions that provide the temporal and spatial evolution of the free surface and the velocity potential, which are the variables describing the motion

of the flow, Laplace's Equation needs to be integrated along with Boundary and Initial Conditions.

3.3.1. Boundary Conditions

There are three different boundary conditions to be defined in this problem: one at the bottom of the channel and two on the free surface. Note that, in an ideal flow, the no-slip boundary condition is lost.

- **No penetration boundary condition**

The no penetration boundary condition states that the velocity component normal to the surface at the bottom of the channel must be zero at every point, at all times. Defining the vector $\vec{N}$ as the unitary vector normal to the bottom surface pointing towards the fluid, $\vec{N} = (0, 0, 1)$, this condition can be formulated as:

$$\nabla\phi \cdot \vec{N} = 0 \tag{3.9}$$

$$\text{at } z = -H.$$

which in turn becomes:

$$\frac{\partial\phi}{\partial z} = \partial_z\phi = v_z = 0 \tag{3.10}$$

$$\text{at } z = -H.$$

- **Kinematic boundary condition**

Refer to Figure 3.1 and let us define the free surface of the water as:

$$F(x, z, t) = z - h(x, t) = 0 \tag{3.11}$$

The kinematic boundary condition imposes that a fluid particle initially on the free surface, stays at all times on the free surface:

$$\frac{DF}{Dt} = 0 \tag{3.12}$$

Using the definition of the substantial derivative:

$$\frac{DF}{Dt} = \partial_t F + \nabla\phi \cdot \nabla F = 0 \tag{3.13}$$

And introducing the expression for F, Equation 3.11, the kinematic boundary condition results in:

$$-\partial_t h - \partial_x \phi \, \partial_x h + \partial_z \phi = 0 \tag{3.14}$$

- **Dynamic boundary condition**

Starting from Bernoulli's Equation (obtained from the Navier-Stokes momentum equation for a flow with no vorticity):

$$\rho \partial_t \vec{v} + \rho \nabla \frac{|\vec{v}|^2}{2} = -\nabla p - \nabla(\rho g z) \tag{3.15}$$

Introducing the previously derived conditions $\rho = constant$ and $\vec{v} = \nabla\phi$, and dividing by density, ρ, Equation 3.15 can be expressed as:

$$\nabla(\partial_t \phi + \frac{1}{2} |\nabla\phi|^2 + p/\rho + gz) = 0 \tag{3.16}$$

This new equation states that the expression between parenthesis is not a function of the position, only of time. Therefore:

$$\partial_t \phi + \frac{1}{2} |\nabla\phi|^2 + p/\rho + gz = f(t) \tag{3.17}$$

If Equation 3.17 is particularized for a fluid particle on the free surface, for which

$$\frac{p}{\rho} = \frac{Pa}{\rho}$$

$$z = H + h$$

it becomes the following Equation 3.18:

$$\partial_t \phi + \frac{1}{2} \mid \nabla \phi \mid^2 + gh = \frac{f(t)}{\rho} - \frac{Pa}{\rho} - gH \tag{3.18}$$

In the equation above, it can be seen that the Left Hand Side depends on the position while the Right Hand Side does not. This fact allows to define the function $f(t)$ in such a way that the RHS becomes zero without affecting in any way the velocity field (since the velocity field remains unaffected if the potential is shifted by a function of the time). After this step, Equation 3.18 finally becomes:

$$\partial_t \phi + \frac{1}{2} \mid \nabla \phi \mid^2 + gh = 0 \tag{3.19}$$

Which is the final statement for the dynamic boundary condition.

3.3.2. Airy Wave Theory

Airy Wave Theory provides the linearized equations that describe the propagation of gravity waves along the surface of an ideal fluid, considering that the mean depth of the propagation domain is constant.

Having defined the governing equations of the flow (Laplace Equation, 3.8) along with the boundary conditions (Equations 3.10, 3.14 and 3.19), linearizing the problem consists in assuming that the amplitude of the oscillations of the free surface is very small. In this way, in first approximation:

- The free surface can be defined as the line $z = 0$.
- The water height can be defined as: $h = \epsilon\, H\, \eta$, where $\epsilon << 1$ and η is a new parameter representing the non-dimensional amplitude of the wave, i.e, $O(\eta) \sim 1$.
- The velocity potential can be expressed as: $\phi = Ux + \varphi\,(x, z)$, where the first term accounts for the uniform velocity field of the unperturbed stream, and the second for the perturbation potential.

- The uniform velocity is non-dimensionalized by means of a characteristic velocity, U_c, such that $\overline{U} = U/U_c$.
- The perturbation potential is linearized as $\varphi = \epsilon\, \phi_c\, \overline{\varphi}\, (\overline{x}, \overline{z})$, where $O(\overline{\varphi}) \sim 1$, $\overline{x}$ and $\overline{z}$ are the non-dimensional x and z coordinates, respectively, and φ_c is a prefactor that contains the order of magnitude of such potential. Note that the problem is planar and it is for this reason that the velocity potential has been expressed only as function of the x and z coordinates and time.
- $\tau = t/t_c$, is the non-dimensional time, such that $O(\tau) \sim 1$.

Using the definitions given above, the variables of the problem and their derivatives can be expressed as:

$$\partial_z \phi = \epsilon\, \varphi_c\, \partial_z \overline{\varphi} = \frac{\epsilon\, \varphi_c}{H}\, \partial_{\overline{z}} \overline{\varphi} \tag{3.20}$$

$$\partial_t h = \frac{1}{t_c} \partial_\tau h = \frac{\epsilon\, H}{t_c}\, \partial_\tau \eta \tag{3.21}$$

$$\partial_x \phi = \frac{\epsilon\, \varphi_c}{H}\, \partial_{\overline{x}} \overline{\varphi} \tag{3.22}$$

$$\partial_x h = \epsilon\, \partial_{\overline{x}} \eta \tag{3.23}$$

$$\partial_t \phi = \frac{\epsilon\, \varphi_c}{t_c}\, \partial_\tau \overline{\varphi} \tag{3.24}$$

$$\nabla \phi = (\partial_x \phi,\ \partial_z \phi) = (\frac{\epsilon\, \varphi_c}{H}\, \partial_{\overline{x}} \overline{\varphi},\ \frac{\epsilon\, \varphi_c}{H}\, \partial_{\overline{z}} \overline{\varphi)} \tag{3.25}$$

$$|\ \nabla \phi\ |^2 = (\frac{\epsilon\, \varphi_c}{H})^2 ((\partial_{\overline{x}} \overline{\varphi})^2 + (\partial_{\overline{z}} \overline{\varphi})^2) \tag{3.26}$$

If these expressions (Equations 3.20 to 3.26) are introduced into the equations derived for the boundary conditions (Equations 3.10, 3.14 and 3.19), the latter become (after some previous mathematical development):

$$\partial_{\overline{z}} \overline{\varphi} = 0 \tag{3.27}$$

$$-\frac{\epsilon H}{t_c}\partial_\tau \eta - U_c\,\epsilon\,\overline{U}\,\partial_{\overline{x}}\eta - \frac{\epsilon\,\varphi_c}{H}\,\partial_{\overline{x}}\overline{\varphi}\,\epsilon\,\partial_{\overline{x}}\eta + \frac{\epsilon\,\varphi_c}{H}\,\partial_{\overline{z}}\overline{\varphi} = 0 \tag{3.28}$$

$$\frac{\epsilon\,\varphi_c}{t_c}\,\partial_\tau\overline{\varphi} + \frac{1}{2}((U_c U + \frac{\epsilon\,\varphi_c}{H}\,\partial_{\overline{x}}\overline{\varphi})^2 + (\frac{\epsilon\,\varphi_c}{H}\,\partial_{\overline{x}}\overline{\varphi})^2) + \epsilon\,g\,H\,\eta = 0 \tag{3.29}$$

Dropping the second order terms (i.e, $O(\epsilon^2)$), Equations 3.28 and 3.29 become:

$$\frac{H}{t_c}\partial_\tau\eta + U_c\overline{U}\,\partial_{\overline{x}}\eta - \frac{\varphi_c}{H}\,\partial_{\overline{z}}\overline{\varphi} = 0 \tag{3.30}$$

$$\epsilon\,\frac{\varphi_c}{t_c}\,\partial_\tau\overline{\varphi} + \frac{1}{2}U_c^2\,\overline{U}^2 + \frac{\epsilon\,U_c\,\overline{U}\,\varphi_c}{H}\partial_{\overline{x}}\overline{\varphi} + \epsilon\,g\,H\,\eta = 0 \tag{3.31}$$

In Equation 3.31, the second term is a constant and therefore can be dropped, as it can be absorbed in the definition of ϕ. Then the expression for the non-dimensional dynamic boundary condition finally becomes:

$$\frac{\varphi_c}{t_c}\,\partial_\tau\overline{\varphi} + \frac{U_c\,\overline{U}\,\varphi_c}{H}\,\partial_{\overline{x}}\overline{\varphi} + g\,H\,\eta = 0 \tag{3.32}$$

In terms of orders of magnitude, from Equations 3.30 and 3.32, one may write:

$$\frac{H}{t_c} = U_c = \frac{\varphi_c}{H} \tag{3.33}$$

$$\frac{\varphi_c}{t_c} = \frac{U_c\,\varphi_c}{H} = g\,H \tag{3.34}$$

Combining these two previous expressions (3.33, 3.34), the orders of magnitude of the characteristic time, velocity and velocity potential are found to be:

$$t_c = \sqrt{\frac{H}{g}} \tag{3.35}$$

$$U_c = \sqrt{gH} \tag{3.36}$$

$$\varphi_c = \sqrt{gH^3} \tag{3.37}$$

At this point and from now on, the non-dimensional velocity of the flume, $\overline{U}$ is:

$$\overline{U} = \frac{U}{U_c} = \frac{U}{\sqrt{gH}} = Fr \tag{3.38}$$

Which is the so called ***Froude number*** and will be explained in more detail in a following section.

Finally, the non-dimensional statement of the problem consists in the non-dimensional Laplace Equation:

$$\partial^2_{\overline{x}\overline{x}}\overline{\varphi} + \partial^2_{\overline{z}\overline{z}}\overline{\varphi} = 0 \tag{3.39}$$

to be integrated with the non-dimensional, linearized boundary conditions (Equations 3.40 - 3.42).

$$\partial_{\overline{z}}\overline{\varphi} = 0 \tag{3.40}$$

$$\text{at } \overline{z} = -1$$

$$\partial_\tau \eta + Fr\, \partial_\tau \eta - \partial_{\overline{z}}\overline{\varphi} = 0 \tag{3.41}$$

$$\partial_\tau \overline{\varphi} + Fr\, \partial_{\overline{x}}\overline{\varphi} + \eta = 0 \tag{3.42}$$

$$\text{at } \overline{z} = 0$$

3.4. Solution to the Homogeneous Linear Problem

In order to solve Equation 3.39 with boundary conditions 3.40 to 3.42, wave-like fundamental solutions were proposed. Any wave can be represented with an exponential function as $\eta\,(x,t) = a\, e^{i\theta\,(x,t)}$, where a is the amplitude and $\theta\,(x,t)$ the phase function (in radians), which depends on the horizontal position and time: $\theta(x,t) = 2\pi(x/\lambda - t/T) = kx - \omega t$.

Thereafter, the non-dimensional flow variables, $\overline{\varphi}$ and η, can be expressed as follows:

$$\overline{\varphi} = f(\overline{z})\, e^{i(\omega\tau - k\overline{x})} \tag{3.43}$$

$$\eta = \eta_0\, e^{i(\omega\tau - k\overline{x})} \tag{3.44}$$

Where $f(\overline{z})$ is a function of the non-dimensional vertical coordinate (since the potential is defined in all the domain and, therefore, it has to depend on all spatial coordinates and time), representing the amplitude of the oscillations of the velocity potential, and η_0 is a parameter representing the amplitude of the oscillations of the free surface.

In what follows, two different analytical methods have been used in order to solve the problem. The first one is a more intuitive approach while the second has a more extended use in the literature and is more rigorous. Different things can be learned from both of them.

3.4.1. A first approach

This first approach consists in obtaining an expression for η in terms of $\overline{\varphi}$ from Equation 3.42, and then introducing it in Equation 3.41 in order to arrive at a single equation in terms of one variable.

First of all, let the following expressions for the derivatives of $\overline{\varphi}$ and η be introduced, since they will result useful in the subsequent analysis.

$$\partial_{\overline{x}}\overline{\varphi} = -i\, k\, f(\overline{z})\, e^{i(\omega\tau - k\overline{x})} \tag{3.45}$$

$$\partial_{\overline{z}}\overline{\varphi} = f'(\overline{z})\, e^{i(\omega\tau - k\overline{x})} \tag{3.46}$$

$$\partial^2_{\overline{x}\overline{x}}\overline{\varphi} = -k^2 f(\overline{z})\, e^{i(\omega\tau - k\overline{x})} \tag{3.47}$$

$$\partial^2_{\overline{z}\overline{z}}\overline{\varphi} = f''(\overline{z})\, e^{i(\omega\tau - k\overline{x})} \tag{3.48}$$

$$\partial_{\tau}\overline{\varphi} = i\,\omega\,f(\overline{z})\,e^{i(\omega\tau - k\overline{x})} \tag{3.49}$$

$$\partial_{\overline{x}}\eta = -i\,k\,\eta_0\,e^{i(\omega\tau - k\overline{x})} \tag{3.50}$$

$$\partial_{\tau}\eta = i\,\omega\,\eta_0\,e^{i(\omega\tau - k\overline{x})} \tag{3.51}$$

Introducing 3.47 and 3.48 into Laplace's non-dimensional equation (Equation 3.39), one arrives to an expression of the form:

$$f''(\overline{z}) - k^2 f(\overline{z}) = 0 \tag{3.52}$$

Equation 3.52 is a homogeneous ordinary differential equation of second order and, therefore, its solution will be of the form $f(\overline{z}) = e^{\alpha\overline{z}}$. Then $f''(\overline{z}) = \alpha^2 e^{\alpha\overline{z}}$. Into Equation 3.52:

$$\alpha^2 e^{\alpha\overline{z}} - k^2 e^{\alpha\overline{z}} = 0 \implies \alpha^2 = k^2 \implies \alpha = \pm k \tag{3.53}$$

Therefore,

$$f(\overline{z}) = C_1\,e^{k\overline{z}} + C_2\,e^{-k\overline{z}} \tag{3.54}$$

Which may also be expressed as:

$$f(\overline{z}) = C_3\cosh(k\,\overline{z}) + C_4\sinh(k\,\overline{z}) \tag{3.55}$$

So that,

$$f'(\overline{z}) = C_3\,k\sinh(k\,\overline{z}) + C_4\,k\cosh(k\,\overline{z}) \tag{3.56}$$

If the expression for $f(\overline{z})$ in 3.55 is introduced in the no-penetration boundary condition, Equation 3.40, this yields:

$$\partial_{\overline{z}}\overline{\varphi} = (C_3\,k\sinh(k\,\overline{z}) + C_4\,k\cosh(k\,\overline{z}))\,e^{i(\omega\tau - k\overline{x})} = 0 \tag{3.57}$$

$$\text{at } \overline{z} = -1$$

Then:

$$C_3\, k \sinh(-k) + C_4\, k \cosh(-k) = 0 \tag{3.58}$$

And therefore, $C_4 = C_3 \tanh(k)$. If C_4 is introduced in the expressions for $f(\overline{z})$ and $f'(\overline{z})$, Equations 3.55 and 3.56, and these are evaluated at $\overline{z} = 0$ (step that will become useful in what follows), one obtains $f(\overline{z} = 0) = C_3/2$ and $f'(\overline{z} = 0) = (C_3/2)\, k \tanh(k)$.

At this point, η can be retrieved from Equation 3.42 as:

$$\eta = -i\, \omega\, f(\overline{z})\, e^{i(\omega\tau - k\overline{x})} + i\, k\, Fr\, f(\overline{z})\, e^{i(\omega\tau - k\overline{x})} \tag{3.59}$$

$$\text{at } \overline{z} = 0.$$

Introducing it into the kinematic boundary condition (Equation 3.41), and dropping the exponential term since it is a common factor different from zero, gives:

$$\omega^2 f(\overline{z}) - \omega\, k\, Fr\, f(\overline{z}) \cosh(k\,\overline{z}) + Fr\, [-\omega\, k\, f(\overline{z}) + k^2\, Fr\, f(\overline{z})] - f'(\overline{z}) = 0 \tag{3.60}$$

$$\text{at } \overline{z} = 0.$$

If the equation above is evaluated, using the values just defined for $f(0)$ and $f'(0)$, it becomes:

$$\frac{C_3}{2}\, \omega^2 - \frac{C_3}{2}\, \omega\, k\, Fr - \frac{C_3}{2}\, \omega\, k\, Fr + \frac{C_3}{2}\, k^2\, Fr^2 - \frac{C_3}{2} k \tanh(k) = 0 \tag{3.61}$$

Which can be rearranged into the following Equation 3.62:

$$\omega^2 - 2\, \omega\, k\, Fr + k^2\, Fr^2 = k \tanh(k) \tag{3.62}$$

Or:

$$(\omega - kFr)^2 = k \tanh(k) \tag{3.63}$$

Which finally brings one to the following relation:

$$\omega = kFr \pm \sqrt{k \tanh(k)} \tag{3.64}$$

Equation 3.64 is the so called ***dispersion relation*** and it is of great interest in the problem because it states that the temporal and spatial frequencies of the waves generated in the channel cannot be independent. This means that, **for a given mean flow in the channel, only those waves whose temporal frequency and wavenumber satisfy the above relationship, will be able to propagate with non-zero amplitude.**

3.4.2. Formal computation of the dispersion relation

This second approach consists in solving the system of equations formed by the non-dimensional boundary conditions in matrix form. The key ingredient of this method is that it formulates the problem as a homogeneous linear system of equations, relating the free constants. The objective is then to find the conditions that would lead to a solution for the system different from the trivial one.

Note that a different notation with respect to the previous approach will be used and now the constants appearing in the expression for $f(\overline{z})$ are called A and B:

$$f(\overline{z}) = A \cosh(k\,\overline{z}) + B \sinh(k\,\overline{z}) \tag{3.65}$$

η is also rewritten as:

$$\eta = C\, e^{i(\omega\tau - k\overline{x})} \tag{3.66}$$

The first derivatives of $\overline{\varphi}$ and η with respect to the non-dimensional spatial coordinates and time, can be computed as:

$$\partial_{\overline{x}}\overline{\varphi} = -i\,(A \cosh(k\,\overline{z}) + B \sinh(k\,\overline{z}))\, k\, e^{i(\omega\tau - k\overline{x})} \tag{3.67}$$

$$\partial_{\overline{z}}\overline{\varphi} = (A\, k \sinh(k\,\overline{z}) + B\, k \cosh(k\,\overline{z}))\, e^{i(\omega\tau - k\overline{x})} \tag{3.68}$$

$$\partial_{\tau}\overline{\varphi} = i\,(A\cosh(k\,\overline{z}) + B\,\sinh(k\,\overline{z}))\,\omega\,e^{i(\omega\tau - k\overline{x})} \tag{3.69}$$

$$\partial_{\overline{x}}\eta = -i\,C\,k\,e^{i(\omega\tau - k\overline{x})} \tag{3.70}$$

$$\partial_{\tau}\eta = i\,C\,\omega\,e^{i(\omega\tau - k\overline{x})} \tag{3.71}$$

Introducing the expressions above into the boundary conditions given by Equation 3.40 (evaluated at $\overline{z} = -1$) and Equations 3.41 and 3.42 (evaluated at $\overline{z} = 0$), one arrives to the following three equations, respectively:

$$-A\,k\sinh(k) + B\,k\cosh(k) = 0 \tag{3.72}$$

$$i\,(\omega - k\,Fr)\,C - B\,k = 0 \tag{3.73}$$

$$i\,(\omega - k\,Fr)\,A + C = 0 \tag{3.74}$$

Which can be rearranged into matrix form as:

$$\begin{bmatrix} -\sinh(k) & \cosh(k) & 0 \\ 0 & -k & i\,(\omega - kFr) \\ i\,(\omega - kFr) & 0 & 1 \end{bmatrix} \cdot \begin{bmatrix} A \\ B \\ C \end{bmatrix} = \vec{0} \tag{3.75}$$

In order for the system to have a solution different than the trivial one (A = B = C = 0), the determinant of the matrix has to be equal to zero. Therefore:

$$k\sinh(k) - (\omega - kFr)^2\cosh(k) = 0 \tag{3.76}$$

Also written as:

$$(\omega - Frk)^2 - k\tanh(k) = 0 \tag{3.77}$$

Which is the exact same expression as Equation 3.63, and therefore will lead to the same dispersion relation found before, Equation 3.64. This last method is more rigorous and more amenable to be extended to more general problems.

As it was previously introduced, the dispersion relation is of great importance in the description of the motion of a gravity wave. In the following section, Equation 3.64 and its implications in the physics of the wave will be explained in detail.

3.5. Dispersion Relation

As it was introduced in Chapter 2, the fact that a wave is dispersive means that its speed of propagation is a function of its wavelength. At this point, we recall that the problem has been linearized and it is homogeneous and, therefore, any solution can be decomposed as a linear combination of fundamental solutions. This means that any arbitrary wave function that is a solution to Equation 3.8 with boundary conditions 3.40-3.42, can be expressed as the superposition of simple harmonic functions (sines and cosines), each of them with a different amplitude, wavelength, initial phase and propagation direction. The wave resulting from the linear combination of fundamental solutions can be therefore understood as a **wave packet** or a **multi-component wave**. The effect of the dispersion relation on such wave packet is that each of the components will propagate with its own phase speed in accordance with Equation 3.64, and therefore, the spatial and temporal properties of the wave envelope will change over time. In order to understand how any initial perturbation on the free surface will propagate in the fluid, one needs to be able to predict how each one of the components that build up the wave describing this initial perturbation varies in time. For this, the **Fourier transform** is a key tool in the analysis.

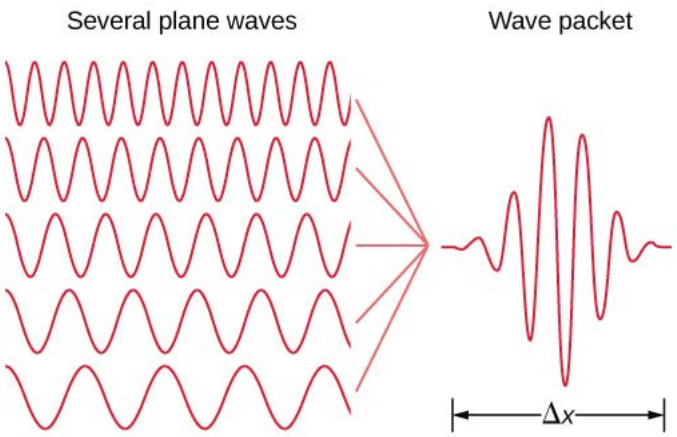

Fig. 3.2. Sketch of a wave packet. [23]

3.5.1. Effect of the Froude number: Doppler shift

Before going into further detail regarding the Fourier analysis of the problem, it is interesting to look at the effect that the Froude number (i.e., the fact that there is a mean flow in the channel before a perturbation appears) has on the propagation of a perturbation.

For a flow in which the mean current is zero, the dispersion relation is not given by Equation 3.64, but by the following Equation 3.78:

$$\omega = \pm \sqrt{k \tanh(k)} \tag{3.78}$$

Comparing both relations,

$$\omega = \pm \sqrt{k \tanh(k)}$$

$$\omega = kFr \pm \sqrt{k \tanh(k)}$$

it can be seen that the waves that propagate in a channel where there is a mean current, experience a Doppler shift, since their frequency of propagation is affected by the velocity of the flow (present in the term kFr). In this way, if the wave propagates in the opposite direction to that of the mean flow, then by the addition of the mean velocity, the wave will propagate slower, i.e, the space it will cover in a given time will decrease. This means that its wavelength will decrease for a given frequency, since recall that the wavelength

is the space travelled by the wave in one period. Accordingly, in the case in which the wave propagates in the same direction as that of the mean current, by the addition of the velocities, the wave components will have an increasing phase velocity, hence a larger wavelength at a given frequency. In conclusion, the Froude number plays a key role in the propagation of a perturbation since it modifies the relation between the frequency and the wavenumber, thus determining which waves can exist, which other cannot, which ones are dragged by the mean flow and which ones can propagate upstream. This is illustrated in the following Figure 3.2. The different graphs show the dispersion relation for different values of the Froude number.

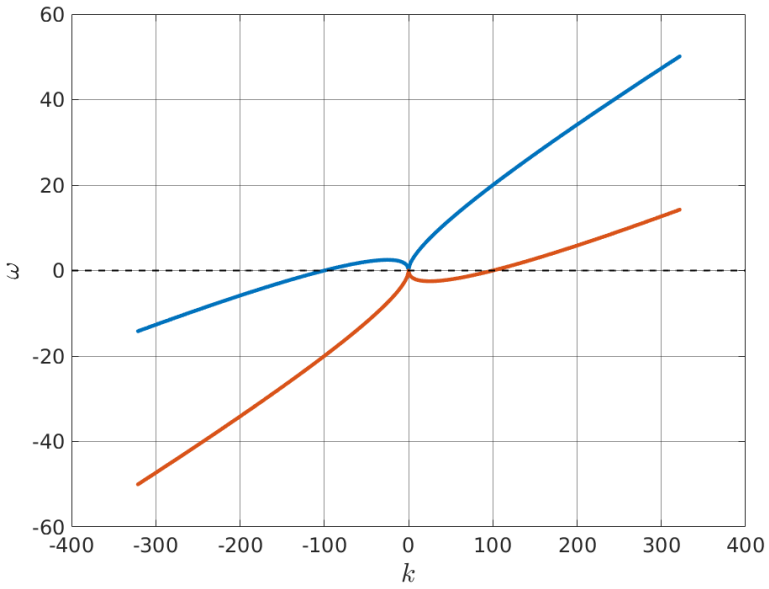

(a)

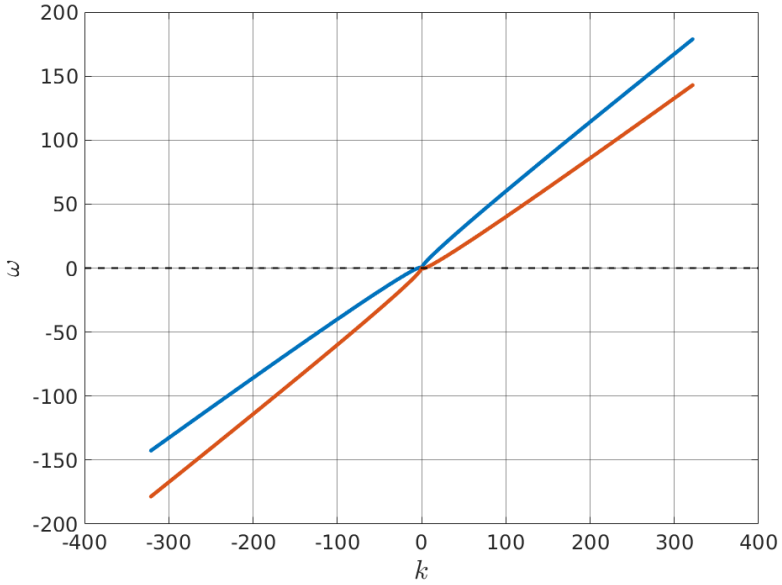

(b)

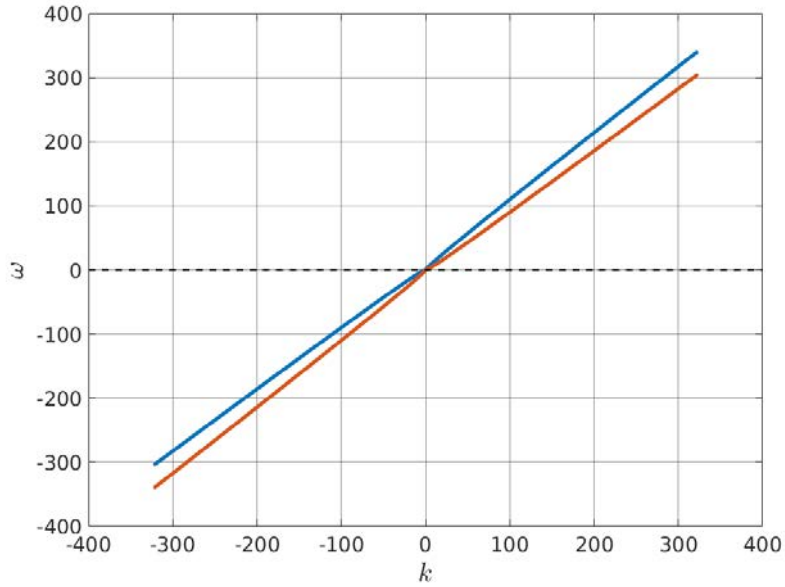

(c)

Fig. 3.2. Dispersion relation for Fr = 0.1, 0.5 and 1, respectively.

Note that, as it can be seen in Figure 3.2, Equation 3.64 has two solutions for ω for a given k due to the square root. This represents the fact that a wave can propagate in both the positive and negative directions of x. Following the expression for the perturbation potential given by Equation 3.43, $\overline{\varphi} = f(\overline{z})\, e^{i(\omega\tau - k\overline{x})}$, the waves with the same sign for

the wavenumber and the angular frequency will propagate to the right, and those having opposite signs for k and ω will propagate to the left. In order to provide a clearer explanation, take for example $Fr = 0.1$ and $k = 50$. From Figure 3.2 (a), one may extract that the two possible angular frequencies for this wavenumber are $\omega_1 = 12$ and $\omega_1 = -2$, approximately. In the next Figure 3.3, what has just been explained above is represented. Indeed, the wave with the same sign for ω and k propagates to the right, and the one with opposite signs for ω and k propagates to the left.

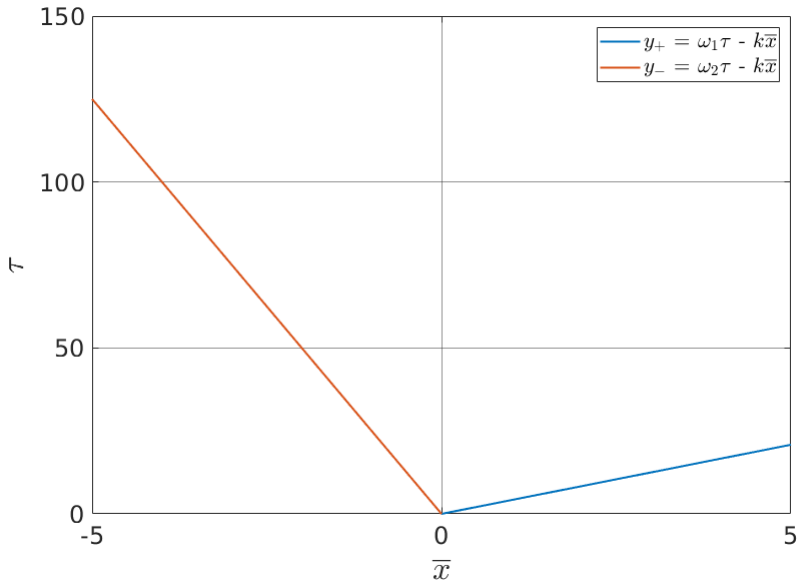

Fig. 3.3. Propagation direction of the waves according to the signs of their wavenumber and angular frequency.

Depending on the flow being simulated, a given wavenumber may be associated to one branch of the angular frequencies or the other. For instance, in order to simulate a wave propagating symmetrically to the left and to the right from the center of the channel as in the present case, one needs to associate to positive (negative) values of the wavenumber, positive (negative) angular frequencies, accordingly. This association is done by means of the sign of the square root in Equation 3.64. In the graphs above, Figure 3.2, the blue curve represents the positive branch of the square root and the orange curve, the negative branch. An important remark is to be done regarding Figure 3.2: note that as the Froude number increases, the curves change in such a way that the two branches come closer to one another. This in turn means that, as the Froude number increases, less waves are able to propagate upstream (to the left) because they get dragged by the

mean current. In order to illustrate this, take again the example for $k = 50$. In Figure 3.2, it can be seen that for $Fr = 0.1$, waves can propagate upstream, as it was shown in Figure 3.3. However, for $Fr = 0.5$, there are no negative angular frequencies for positive wavenumbers and viceversa, i.e, waves cannot propagate to the left anymore. Actually, for $Fr \geq 0.5$, the graphs represent a situation in which, for positive wavenumbers, only positive angular frequencies exist, and similarly for negative wavenumbers and negative angular frequencies. Following the explanation given above, this means that only waves propagating to the right can exist in the channel as the Froude number increases. In other words, as the mean current velocity increases, waves cannot overcome it and they all get dragged by it. As a final remark to entirely understand the influence of the Froude number in the propagation of the waves, think of the ideal case in which $Fr \to \infty$. See that in Equation 3.64, and following the behaviour described by the graphs in Figure 3.2, in this limit, the term of the square root is lost and only the linear contribution of k would play a role in the value of ω, which would be represented as a single straight line. In this is the case the wave is only carried away by the fluid and no waveis able to propagate upstream.

3.6. Fourier Analysis

A monochromatic wave is a wave with a single wavelength (a single color): a pure wave. This type of wave is really an idealization: on the one hand, because being a periodic process both in space and time, it should propagate infinitely in space and have an infinitely large duration in time, two points that are obviously not attainable. On the other hand, because there do not exist in nature pure monochromatic wave emitters: every emission process has a damping associated to it which is translated into the emission of frequencies different from the central or carrier frequency. Consequently, a real undulatory process is a result of the superposition or interference of several monochromatic waves [24]. It is at this point where the Fourier Analysis is introduced.

The Fourier transform maps a function from the time or the space domain into the frequency domain. Similarly to what happens when one projects a three-dimensional vector into the Cartesian coordinate basis (for instance), when one projects a function into the Fourier space, this function is decomposed as a linear combination of the fundamental components of the basis of the Fourier space, each of them multiplied by a factor, named

Fourier coefficient. The fundamental components of the Fourier space are the simplest possible waves, the sine and cosine waves, along the infinite frequency spectrum. One may notice that, in contrast to the previous example of the Cartesian coordinate basis, the Fourier space is formed by an infinite basis. Projecting a function into the Fourier space provides the frequency components of the function. The interest in decomposing a function into its frequency components (the simple sine waves that form it) lies in the fact that it is much simpler to analyze the evolution of each of the components rather than the evolution of the wave as a whole. This may be better understood with the following Figure 3.4: the functions $f(t_1)$ and $f(t_2)$ are much more simple to represent and study than their superposition. The lowest plot shows the frequency components of the total wave. (Note that the functions in the figure depend on time and not on space, but the analysis is similar and for the purpose of understanding, equally valid).

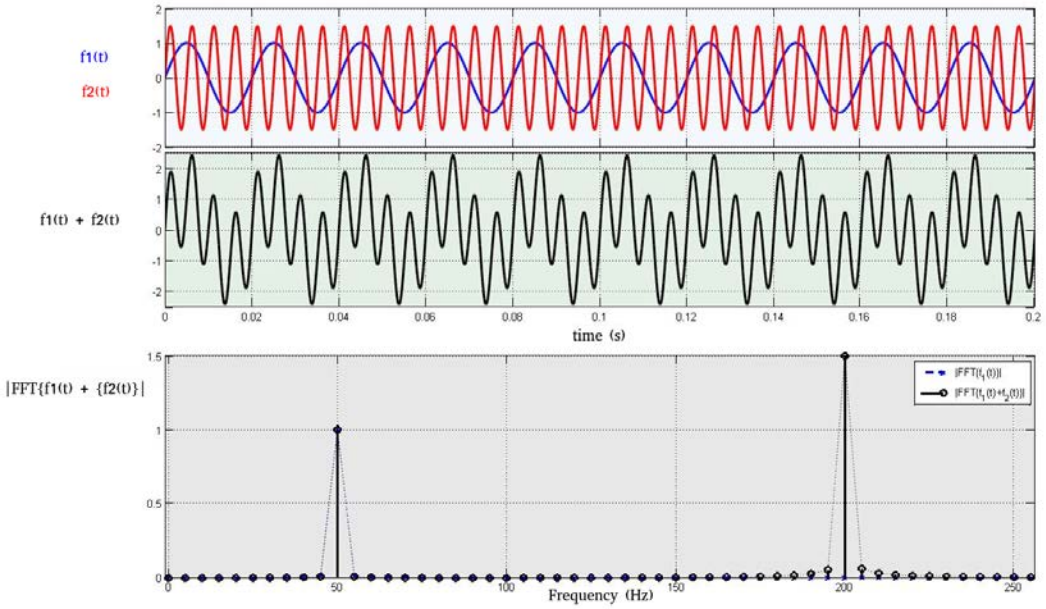

Fig. 3.4. Sketch illustrating the interpretation of the Fourier transform. [25]

As it was introduced above, the Fourier transform of a function yields its frequency components and a coefficient associated to each of them. Similarly to the situation of projecting a vector in the Cartesian coordinate basis, each of these coefficients represents the intensity of its associated frequency in the whole solution. The Fourier coefficients are the amplitude of the sinusoidal wave at the corresponding frequency.

Mathematically, the Fourier transform is performed by means of the following expres-

sion:

$$\hat{f}(\xi) = \int_{-\infty}^{\infty} f(x) e^{-i2\pi\xi x} dx \tag{3.79}$$

where x is the spatial coordinate and ξ the spatial frequency.

If one analyzes the above expression, its usefulness can be seen straightaway: knowing that the notation $e^{i2\pi\xi_0 x}$ is used to represent a wave with zero initial phase and frequency ξ_0 as introduced in Section 3.4, note that the negative sign of the exponential term of the Fourier transform will cause its product with the wave under analysis, $e^{i2\pi\xi_0 x}$, be equal to one when $\xi = \xi_0$. This will result in the integral diverging, yielding the Dirac delta function at $\xi = \xi_0$: exactly the result aimed for since this is the only frequency component of the sinusoidal wave $e^{i2\pi\xi_0 x}$. In this way, the Fourier transform "unmasks" all the frequencies comprised in a function.

The Fourier coefficient of each frequency is found by evaluating Equation 3.79 at the corresponding frequency. The function $f(x)$ can be reconstructed from its transformed in the frequency domain through the *inverse Fourier transform*:

$$f(x) = \int_{-\infty}^{+\infty} \hat{f}(\xi) e^{i2\pi\xi x} d\xi \tag{3.80}$$

Note that Equation 3.79 gives the Fourier transform of a generic non-periodic function, and it is for this reason that the integration domain extends from $-\infty$ to $+\infty$: non-periodic functions can only be mapped into the continuous frequency domain in order to be completely determined. The situation is different, however, for periodic functions. The latter can be expressed as a discrete superposition of sine waves in an interval (the period of the function). Thus a periodic function in the space (or time) domain can be reconstructed from its frequency components by means of a series (*Fourier Series*) rather than an unbounded integral as:

$$f(x) = \sum_{-\infty}^{+\infty} c_n e^{i2\pi n x/L} d\xi \tag{3.81}$$

where c_n are the Fourier coefficients, defined as:

$$c_n = \frac{1}{L} \int_{-\frac{L}{2}}^{+\frac{L}{2}} f(x) e^{-i2\pi nx/L} d\xi \tag{3.82}$$

and L is the spatial period.

Nonetheless, there is a close relation between the definition of the Fourier series given by 3.81 and that of the Fourier transform, given by 3.79, for a function that is zero everywhere except at a given interval. For such a function, one can define both the Fourier transform and the Fourier series, considering for the last case an interval that includes all the points in which f is not zero. As the interval in which the Fourier series is calculated increases, the Fourier coefficients of the series start to resemble the Fourier transform evaluated at each given frequency, and the sum of the Fourier series of f starts to resemble the inverse Fourier transform (Equation 3.80). In fact, assume that the period, L, of this function f is such that the interval being considered completely contains the interval $[-L/2, L/2]$ in which f is different from zero. If one compares the definition of the Fourier series coefficients, Equation 3.82, with that of the Fourier transform, Equation 3.79, and because f is zero at all points outside the interval $[-L/2, L/2]$, then it is derived that:

$$c_n = \frac{1}{L} \hat{f}(\frac{n}{L}) \tag{3.83}$$

All in all, for a function different from zero only in some interval $[-L/2, L/2]$, the Fourier coefficients are found to be the values of the Fourier transform sampled on a grid of width $1/L$ and multiplied by this grid width. Understanding this last point is of great use in the present analysis, since the initial condition of our problem is precisely a function defined in some particular interval, namely, the channel. An interesting remark to be made at this point is the relationship between the spatial width of this initial condition in the given interval and the number of frequencies (and therefore, coefficients) that are needed to represent it in the frequency domain. Given the domain we have been using up to now, $[-L/2, L/2]$, the lesser the periods the initial condition completes in this domain, the wider its Fourier transform will be in the frequency domain, i.e, the more coefficients it will need to be completely described. Similarly, in the opposite case, the higher the number of periods the initial perturbation completes in the given interval, the narrower

its Fourier transform will be. The reason is that, when the function completes a lot of periods in the selected interval of the space (or time) domain, it can be represented with high accuracy with just one frequency: it is as if just one single frequency defined the pulse. However, take for example that the function completes only two periods in the space (or time) domain. Then it is difficult to determine the exact point at which one period finishes and the new one starts. In this latter situation, a high amount of harmonics needs to be used in order to reconstruct the wave with enough accuracy. Let us illustrate this with an example using the following function given by a Gaussian times a sine wave, Equation 3.84:

$$f_0(x) = e^{-x^2/W^2} \sin(2\pi\, f_c\, x); \tag{3.84}$$

where W is the width of the Gaussian function and f_c is the central or carrier frequency of the pulse.

In the following Figures 3.5 and 3.6, the phenomena just described above is clearly represented: in Figure 3.5 (a), the width of the Gaussian has been set to $W = 0.2$. Correspondingly, the initial condition in this case is a narrow pulse in the space domain, which is translated into a wide spectrum of frequencies in the frequency domain, Figure 3.6, (a). In contrast, in Figure 3.5 (b), the width of the Gaussian is $W = 2$, and the initial condition needs just a few Fourier coefficients to be completely represented in the frequency domain, Figure 3.6 (b).

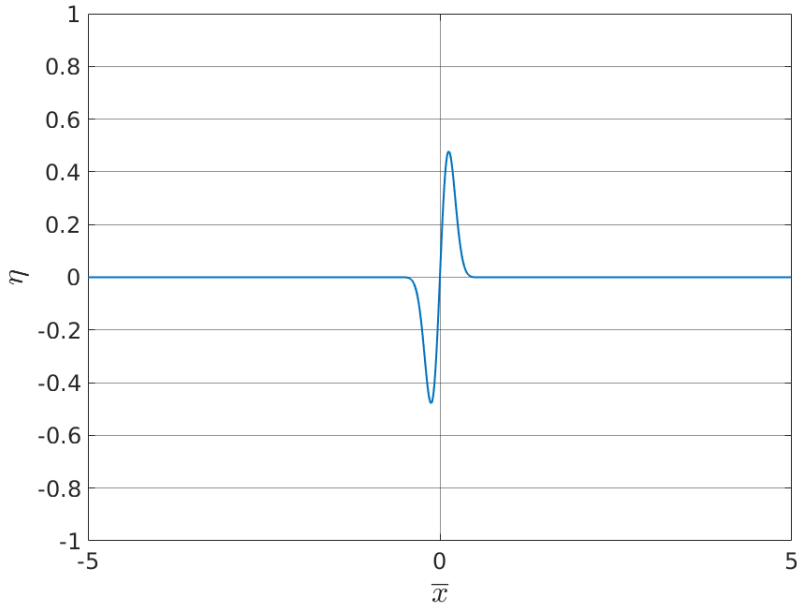

(a)

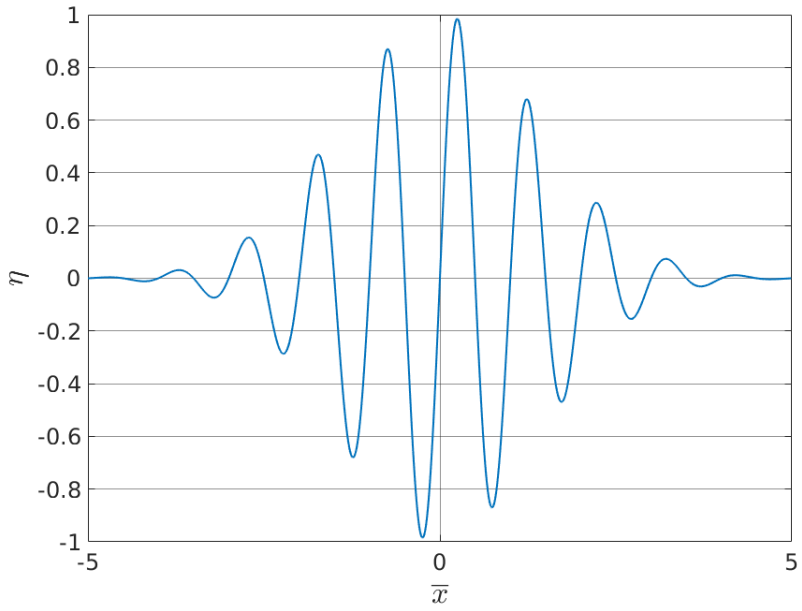

(b)

Fig. 3.5. Initial condition for different widths of the Gaussian: (a) W = 0.2, (b) W = 2.

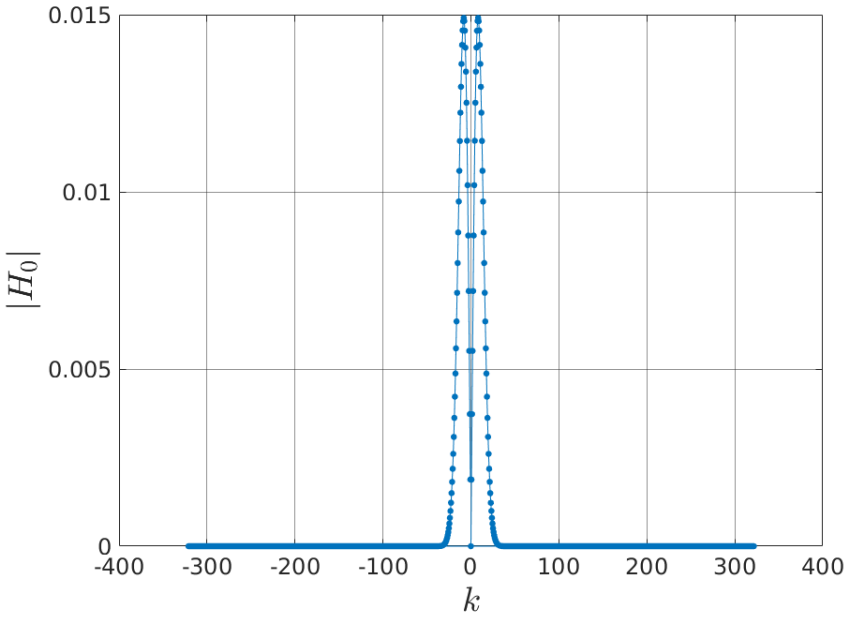

(a)

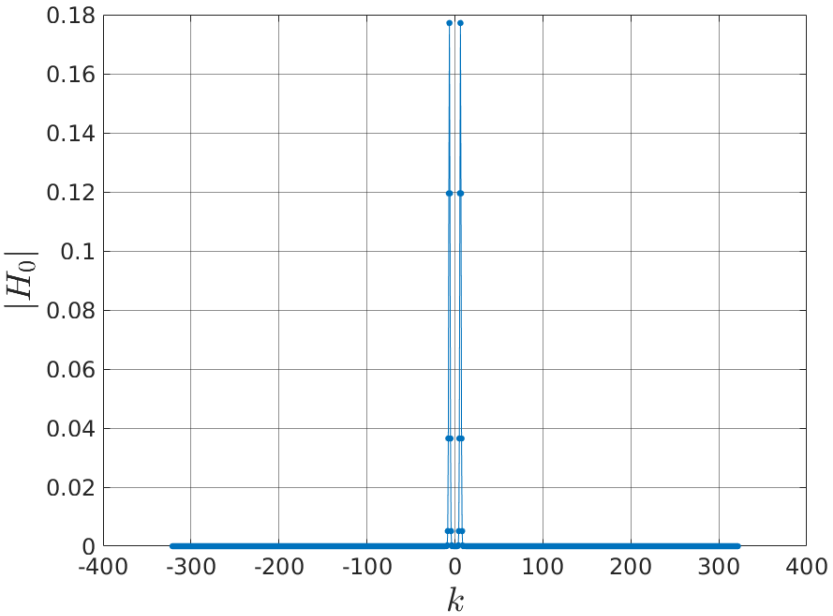

(b)

Fig. 3.6. Fourier coefficients of the initial condition with different widths of the Gaussian: (a) W = 0.2, (b) W = 2.

The Fourier coefficients of the initial condition, which are essential in order to understand the evolution of this condition in time, can be obtained by means of the procedure described above, through Equation 3.82. The function that was used as initial condition

for the homogeneous linear problem consists in a simple Gaussian function:

$$\eta_0(\overline{x}) = 1 + 2\,\epsilon\, e^{-\frac{\overline{x}^2}{W^2}} \tag{3.85}$$

where $\overline{x} \in [-5, 5]$, ϵ is a parameter such that $\epsilon << 1$ in order to make the amplitude of the initial condition small, in particular, $\epsilon = 0.1$, and the width of the Gaussian has been set to $W = 2$.

Even if this wave shape has an analytical Fourier transform, the Fourier coefficients have been obtained by means of MATLAB in order to be able to change arbitrarily this initial condition easily. MATLAB is able to obtain the Fourier coefficients of a given input implementing the described method through its built-in functions *fft* or *ifft*, depending on the input.

At this point, the reader may have noticed that this procedure was introduced in order to find the evolution of the initial condition with time, nevertheless, time has not appeared in the derivation up to this point.

Note that the wave appearing in the definition given for the Fourier transform, Equation 3.79, does not have exactly the same form as that used in Section 3.4 as a solution to the problem under study. The difference is that the latter depends also on time. Therefore, when performing the Fourier transform of $\eta\,(\overline{x})$, the exponential term depending on time, $e^{i\omega\tau}$, can be extracted out of the integral, since it does not depend on $\overline{x}$, in such a way that the Fourier coefficients of the present case can be defined as:

$$c_n(\tau) = \frac{e^{i\omega_n\tau}}{L}\hat{f}(\frac{n}{L}) \tag{3.86}$$

This relation determines the time evolution of the Fourier coefficients. It is important also to remark that not only each Fourier coefficient depends on time, but this evolution is determined by its angular frequency, ω_n, which, as given by the dispersion relation, Equation 3.64, depends on its associated wavenumber, k_n. This means that each Fourier coefficient will vary in a particular way determined uniquely by the frequency it is representing, i.e, each frequency component varies differently in time.

3.7. A channel with variable depth: Shallow Water Theory

After we have seen the analytical approach to the simpler case of a straight channel, in order to study the evolution of the flow when the channel presents a bottom topography, some changes need to be done on such theoretical analysis. In particular, the presence of the bottom topography introduces a new dependency of the flow parameters on x that makes the problem no longer homogeneous. Consequently, the so-called Shallow Water Theory needs to be used as opposed to Airy Wave Theory.

The Shallow Water equations are derived from the Navier-Stokes equations after taking into account some considerations, mainly: considering the variable depth of the channel, assuming that the horizontal flow velocity is constant with the depth, and neglecting the viscosity and the surface tension [26]. As a result, these equations describe the flow field below a surface of pressure (in this case the free surface of water), in terms of the free surface depth, $h(x)$, and the horizontal velocity of the flow.

See Figure 3.7 to picture the new problem geometry.

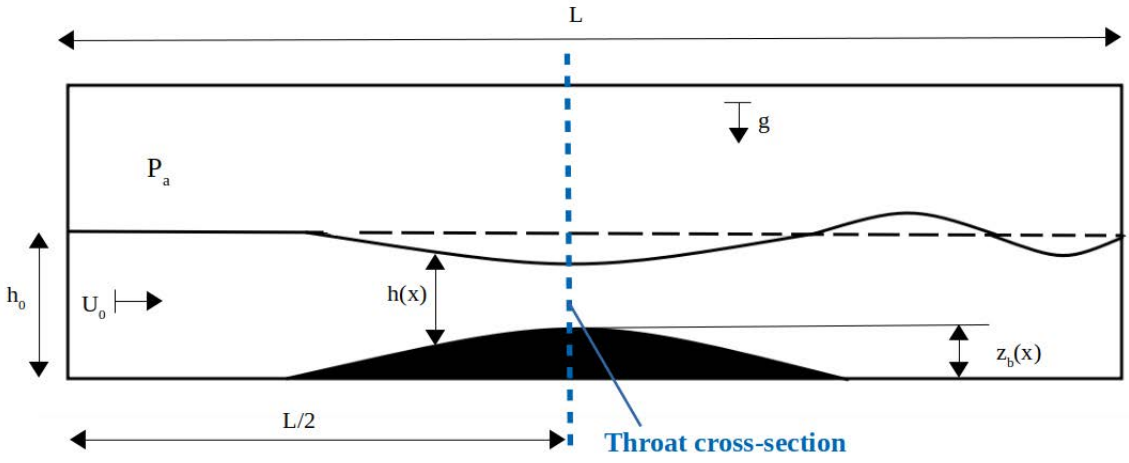

Fig. 3.7. Sketch of a channel with a bottom topography.

The main equation of the Shallow Water Theory, which gives the relation between the depth of the free surface of water, the bottom height and the horizontal flow velocity, can be obtained as follows:

Let $q(x)$ be the mass flux through a vertical line at a given x coordinate (recall that the problem is planar in the xz plane), $q(x) = U(x)\,h(x)$, where $U(x)$ is the horizontal

velocity of the flow and $h(x)$ is the depth of the free surface with respect to the bottom at that x. Since the flow is assumed to be ideal and steady, Bernouilli's Equation (3.15), can be applied on the free surface, yielding:

$$p_a + \frac{1}{2}\rho U_0^2 + \rho g h_0 = p_a + \frac{1}{2}\rho U(x)^2 + \rho g\left(h(x) + z_b(x)\right) \tag{3.87}$$

where the subindex 0 is assigned to the variables at $x = 0$, and z_b stands for the height of the bottom at a given x coordinate. Rearranging the previous equation and introducing the definition given above for the mass flux, $q(x)$:

$$\frac{1}{2}U_0^2 + g h_0 = \frac{q^2}{2h^2} + g(h + z_b) \tag{3.88}$$

Dividing this equation by $g h_0$, one arrives to:

$$\frac{1}{2}Fr_0^2 + 1 = \frac{Fr^2}{\bar{z}_h^2} + \bar{z} + \bar{z}_b \tag{3.89}$$

where $\bar{z}_h = h/h_0$, $\bar{z}_b = z_b/h_0$ are new non-dimensional parameters representing the depth of the free surface of water and the bottom's height, respectively, and Fr represents the Froude number, as already defined earlier in this report.

Solving Equation 3.89 for $\bar{z}_b$ allows to visualize in a clearer way the dependency between these three parameters: given the height of the bottom topography at each x coordinate, the solution to the problem consists in finding the horizontal velocity and the free surface depth that satisfy Equation 3.90 at that x.

$$\bar{z}_b = \frac{1}{2}Fr_0^2\left(1 - \frac{1}{\bar{z}_h{}^2}\right) + 1 - \bar{z}_h \tag{3.90}$$

Equation 3.90 illustrates how the presence of a topography at the bottom of the channel displaces the free surface of water in such a way that, as the bottom height increases, the depth of the free surface decreases. The reason is that the increase of the bottom height has two consequences on the flow above it: first, an increase of the hydrostatic pressure, and second, a reduction of the cross-sectional area of fluid. For flows in subcritical conditions as it is the case here, the effect of the area reduction is more significant than the increase of the hydrostatic pressure. As a result, since mass has to be conserved, given $q(x) =$

$U(x)\,h(x)$, as the bottom rises, the 2D cross-sectional area, $h(x)$, decreases, which makes the horizontal velocity increase. If the flow is accelerated, the pressure decreases making the free surface of water descend, reaching its minimum value at the x coordinate in which the bottom height is maximum. Let us denote the cross-section at which this occurs as the *throat* of the channel. Note that this explanation applies only to the region before the maximum bottom height. As we shall see later, after the flow has passed the obstacle, the free surface of water may follow different behaviours depending on the horizontal velocity of the flow.

3.7.1. Reaching critical conditions: $Fr = 1$ at the throat

Equation 3.90 allows us to arrive to another important result: the value of the maximum height that will make $Fr = 1$ at that x coordinate for a given Fr_0. The derivation of such values provides us with important information and it is as follows.

On the one hand, if one takes the derivative of Equation 3.90 with respect to $\overline{z}_h$ and equals it to zero, it is found that the maximum of such function $\overline{z}_{b,max}$ is at $\overline{z}_{h,c} = Fr_0^{2/3}$.

On the other hand, following the definition of the Froude number, the *critical* Froude number is given by, $\tilde{Fr} = U_c/\sqrt{gh_c} = 1$. Using the definition of the mass flux given before, $q = U_0\,h_0 = U_c\,h_c$:

$$\tilde{Fr} = \frac{U_c}{\sqrt{gh_c}} = \frac{U_0\,h_0}{h_c\,\sqrt{gh_c}} = \frac{U_0}{\sqrt{gh_0}}\,h_0^{3/2}h_c^{-3/2} \tag{3.91}$$

So that, finally, $\tilde{Fr} = Fr_0\,\overline{z}_{h,c}^{-3/2} = 1$. And, therefore, $\overline{z}_{h,c} = Fr_0^{2/3}$.

The two conditions given above imply that the x coordinates at which the bottom height is maximum and the Froude number is critical are actually the same. Therefore, $Fr = 1$ at $\overline{z}_{b,max}$.

Following this, if one introduces the maximum height of the bottom, $\overline{z}_{b,max}$ in Equation 3.90 with the corresponding value of the free surface depth, $\overline{z}_h = Fr_0^{2/3}$, the following equation in terms of only Fr_0 is obtained:

$$\overline{z}_{b,max}(x) = \frac{1}{2}Fr_0^2\left(1 - \frac{1}{Fr_0^{4/3}}\right) + 1 - Fr_0^{2/3} \tag{3.92}$$

which will lead to the value of the Froude number that the flow needs to be given at the beginning of the channel in order to reach critical conditions at the throat. In this case, the bottom topography was defined by means of the following function, because it provides a gradual increment of the bottom surface and it reaches a convenient maximum height:

$$\overline{z}_b\left(\overline{x}\right) = 0.3\, e^{-\frac{(\overline{x}-10)^2}{4}} \tag{3.93}$$

for which the maximum is $\overline{z}_{b,max} = 0.3$. Introducing this value in Equation 3.92, the initial Froude number required for the flow to be critical at $\overline{z}_{b,max} = 0.3$ is $Fr_0 = 0.3655$, and the corresponding water depth, $\overline{z}_{h,c} = 0.5112$, approximately. Note that whole derivation done above takes into account strong assumptions that greatly simplify the problem, therefore, these values are not exactly the ones that would be obtained in a real experiment, but they work as a first approximation and in order to implement the numerical simulation.

3.7.2. Free surface of water: convergent-divergent nozzle analogy

As it was introduced earlier, the value of the horizontal velocity determines the position of the free surface after it has passed the obstacle. If the value of the local Froude number of the flow is close but smaller than one as the flow approaches the throat, the free surface of water will go back to its initial configuration symmetrically with respect to the vertical line passing through the throat. In contrast, if the local Froude number before the throat is slightly greater than one, once the maximum point is passed, the flow will reach supercritical conditions, its pressure will decrease significantly and the depth of the free surface will decrease accordingly. The reason is that the critical point is unstable and the flow will always tend to return to the region it was before reaching it.

The whole situation can be explained by means of an analogy with the convergent-divergent nozzle of an aircraft. Let us support this explanation with Figures 3.8 and 3.9:

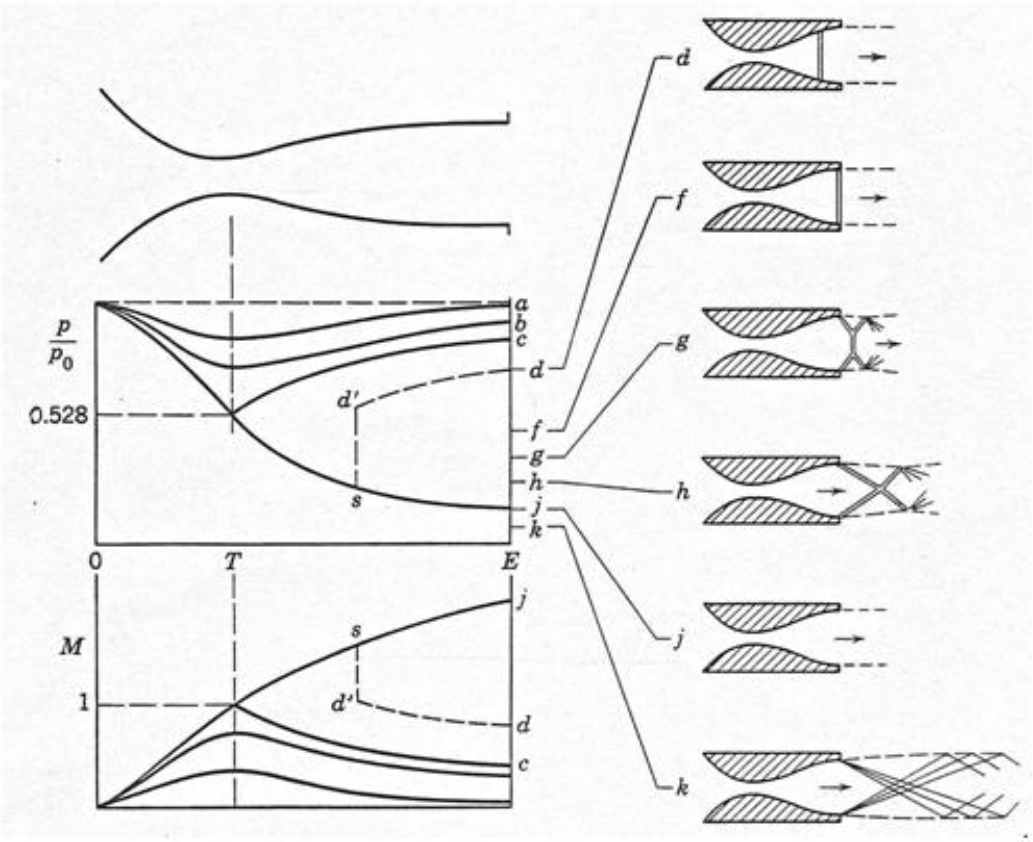

Fig. 3.8. Flow in a convergent-divergent nozzle. [27]

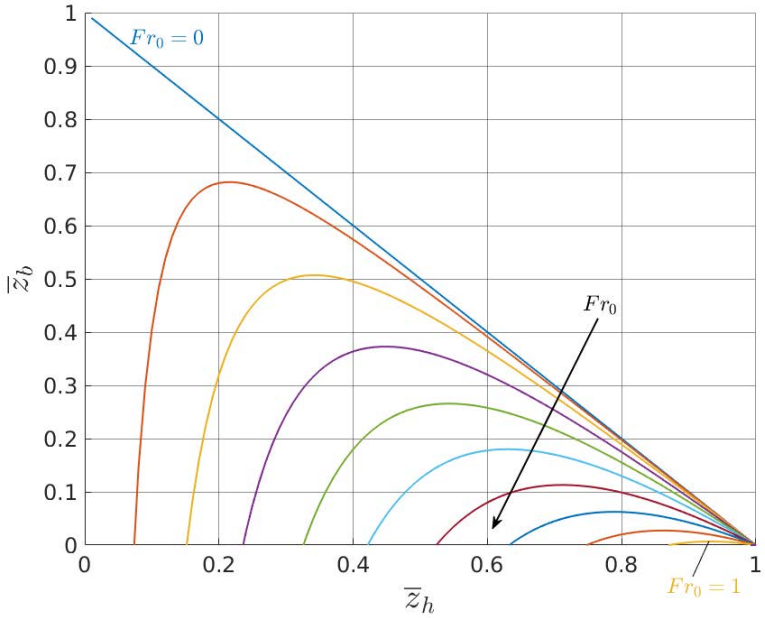

Fig. 3.9. Variation of the water depth with the bottom height for different values of Fr.

Refer first to Figure 3.8. The different curves show the behaviour of the pressure of the

flow as it travels along the nozzle, depending on the value of the external pressure. The flow accelerates in the convergent part of the nozzle and it expands (and therefore, decelerates) in the divergent section. As the external pressure decreases, the flow accelerates more in the convergent zone up to the limiting point in which it reaches sonic conditions at the throat (b), which is the section of minimum area, and therefore, maximum velocity. In this situation, we say the throat is *choked*. From this value of the external pressure on, the throat remains always choked. As the external pressure keeps decreasing, the divergent section does not expand the flow enough to lower its pressure down to the external one, thus, a normal shock wave appears inside the nozzle in order to decrease the pressure to the required external value (c - e). This is the case until f, in which the evolution of the flow is isentropic and it exits as a supersonic jet (i.e, the value of the internal pressure is exactly that of the external one). For case g, the value of the pressure of the flow at the exit is actually smaller than the external one and therefore, the flow undergoes an expansion (*Prandtl-Meyer expansion*).

The cases of use to establish an analogy with the channel are a and f. In both, the evolution of the flow is isentropic along the entire nozzle and sonic conditions are reached at the throat. The difference between both cases lies in the value of the Mach number just before the throat. The Mach number is a non-dimensional parameter representing the ratio between the flow velocity and the speed of sound in a given media, and it is analogous to the Froude number for the flow in the channel. In case a, the flow is subsonic before the throat and therefore, after reaching sonic conditions at the throat, it continues to be subsonic afterwards. In case f, the flow accelerates up to a value of the Mach number slightly higher than one in the convergent section, and so after passing the throat at sonic conditions, it continues in the divergent region in supersonic conditions. In this latter scenario, since the flow is supersonic (higher velocity), its pressure is much smaller than that for case a. These two situations represent exactly the two possible solutions for the free surface depth after passing the maximum height in the channel.

At this point, refer to Figure 3.9, where Equation 3.90 has been plotted for different values of the initial Froude number. It can be seen that as $\overline{z}_h$ increases, $\overline{z}_b$ increases until it reaches its maximum value. This maximum height decreases with increasing Fr_0. This makes sense since, as explained above, at the point of maximum height, the Froude number becomes critical. As the initial Froude number of the flow increases, the starting

point of the flow is closer to $\tilde{Fr} = 1$ and therefore, it will need to be less accelerated to actually reach $\tilde{Fr} = 1$.

In relation to Figure 3.8, for each $\overline{z}_b$, there are two solutions for $\overline{z}_h$ (as for the case of isentropic flow in the nozzle). This represents the two different behaviours the free surface can follow. If after the top of the obstacle, $\overline{z}_h$ is the greater solution, it means that the flow was subsonic right before the maximum point and the free surface will recover its depth symmetrically as the bottom height decreases. If $\overline{z}_h$ is the smaller value, it means that the flow is in supercritical conditions after it has passed the obstacle. The situation of interest in this study is the first one because if the flow is supercritical and the free surface descends, the initial perturbation will not even be able to reach the throat and the pair-wave creation will not be observed. In contrast, if the free surface regains the shape it had before the obstacle, the initial perturbation takes place at a region where the flow is in subcritical conditions. Consequently, when it reaches the critical region at the throat, it does not have enough kinetic energy to penetrate into it and it is blocked. Given that the total momentum and energy of the system have to be conserved (except for non-conservative effects that take place in a real facility, such as viscous dissipation), when the incoming wave is blocked it rebounds into two short waves that propagate in the opposite direction with amplitudes and frequencies such that both momentum and energy are preserved.

4. NUMERICAL SIMULATION.

As it was introduced at the beginning of this report, the first objective regarding the numerical simulations is to obtain the evolution of an linear initial condition in a straight channel in which there is a mean flow. The results of such simulation are to be compared with those obtained from the Airy Wave Theory, Section 3.4 of Chapter 3, in order to verify the validity of the computational methodology. It is needed to stress the great practical importance of this step since, once the validity of the numerical procedure is proven, one can increase the complexity of the problem for the numerical simulation in order to obtain a reliable description of the behaviour of the fluid under conditions for which an analytical solution is not possible or has not been found yet. One of such cases is precisely the evolution of a flow in a channel with a bottom topography and a mean current. Therefore, once the correlation between the analytical and the numerical results for the linear problem has been successfully checked, the topography will be introduced in the numerical domain and the evolution of the flow under the conditions described in the Section 3.7 of Chapter 3 will be study with a new simulation, following the same computational methodology.

As it has already been mentioned, the software used in order to perform the simulations was *Gerris*, for which an introductory description will be given in the next section.

4.1. Introduction to the software: *Gerris*.

Gerris is a CFD software developed by Stéphane Popinet and supported by the Institut Jean le Rond d'Alembert. The software is open-source and can be acquired for free under the requirements of the GNU General Public License. Popinet introduced and described *Gerris'* features for the first time in two different articles published in the *Journal of Computational Physics* in 2003 and 2009, named, respectively "*Gerris: a tree-based adaptive solver for the incompressible Euler equations in complex geometries*" [28] and "*An accurate adaptive solver for surface-tension-driven interfacial flows*" [29]. In what follows, the most remarkable features of *Gerris* will be introduced. Note that *Gerris* solves both 2D and 3D flows but since the flow under study is planar, only the features for 2D flows

will be described.

- **Spatial discretization.** The domain is discretized by means of square finite volumes, each of them called a *cell*, that are organized hierarchically as a quadtree, as shown in Figure 4.1.

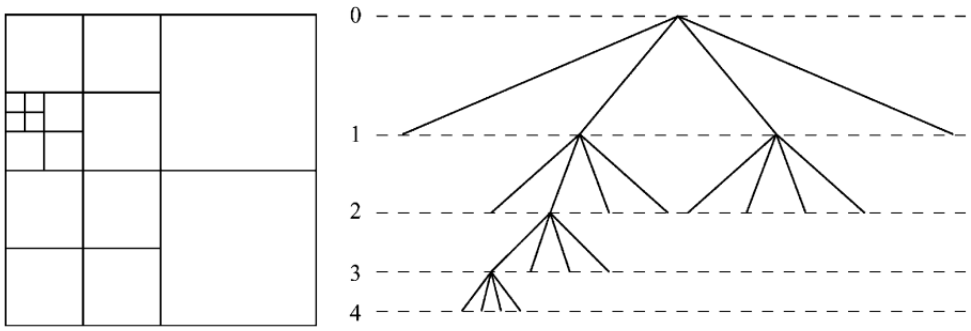

Fig. 4.1. Quadtree discretization and corresponding tree representation. [28]

Each cell can be the *parent* cell of up to four *children*. The first cell of the domain is the *root cell*, and it is the base of the tree. A cell without any children is called a *leaf cell*. The *level* of each cell is defined by adding one to the previous level, where the level zero is that corresponding to the root cell. In a 2D domain, each cell has a direct neighbouring cell in every direction of its same level. Those cells that are cut by a solid boundary are called *mixed cells*. In order to simplify the calculations of the gradient and the flux of the variables, the discretization of the domain is subjected to two main constraints, namely: the levels of direct and diagonally neighbouring cells cannot differ by more than one and those cells that are neighbours of a mixed cell must be at the same level.

- **Adaptive mesh refinement.** The spatial discretization is adjusted dynamically to the scale and temporal evolution of the flow features.

- **Volume-of-Fluid interface representation.** The VOF method provides a robust and efficient representation of the interface as it evolves, even for complex topologies. The fact that *Gerris* combines the VOF representation with the adaptive quadtree spatial discretization allows the resolution along the interface to vary. This constitutes a break point with respect to previous methods in which the resolution

for the interface was fixed, and only in regions far from it the resolution was allowed to adapt.

- **Flow variables.** All the flow variables are defined at the center of each of the cells. This definition simplifies the conservation of momentum in relation to the adaptive mesh. Following the finite-volume discretization, the variables at each cell are interpreted as the volume-average values for the corresponding discretization volume.

- **Governing equations and numerical scheme.** *Gerris* solves the incompressible, variable-density, Navier-Stokes equations with surface tension:

$$\rho(\partial_t \vec{u} + \vec{u} \cdot \nabla \vec{u}) = -\nabla p + \nabla \cdot (2\mu \vec{D}) + \sigma k \delta_S \vec{n} \tag{4.1}$$

$$\partial_t \rho + \nabla \cdot (\rho \vec{u}) = 0 \tag{4.2}$$

$$\nabla \cdot \vec{u} = 0 \tag{4.3}$$

  where $\vec{u} = (u, v, w)$ is the fluid velocity, $\rho \equiv \rho(\vec{x}, t)$ is the fluid density, $\mu \equiv \mu(\vec{x}, t)$ is the dynamic viscosity and $\vec{D}$ the deformation tensor. The Dirac distribution function δ_S states that the surface-tension term is concentrated on the interface, σ is the surface-tension coefficient, and κ and $\vec{n}$ the curvature and normal to the interface.

  The numerical scheme implemented is based on the previously explained quadtree spatial discretization, a multilevel Poisson solver, an approximate projection method and a momentum advection scheme.

- **Two-phase flows.** The density and viscosity fields for two-phase flows are defined in terms of the volume fraction $c(\vec{x}, t)$ of the first fluid as:

$$\rho(\tilde{c}) \equiv \tilde{c}\rho_1 + (1 - \tilde{c})\rho_2 \tag{4.4}$$

$$\mu(\tilde{c}) \equiv \tilde{c}\mu_1 + (1 - \tilde{c})\mu_2 \tag{4.5}$$

  where ρ_1, ρ_2 and μ_1, μ_2 are the density and viscosity of the first and second fluid, respectively, and $\tilde{c}$ is the variable c with a spatial filter applied.

- **Advection equation.** The advection equation in the case of two-phase flows can be defined for the volume fraction c instead of for the density as:

$$\partial_t c + \nabla \cdot (c\vec{u}) = 0 \tag{4.6}$$

- **Temporal discretization.** The temporal discretization is done by means of a staggered method for the volume fraction and the pressure that leads to a second-order accurate system which is simplified through a time-splitting projection method. The solution is then obtained solving iteratively a Poisson equation.

4.2. Numerical set-up: a straight channel

Gerris is designed to work with non-dimensional variables, therefore, the Navier-Stokes equations (4.1 - 4.3) were made non-dimensional for both the water and the air, taking as non-dimensionalizing variables: the water height of the still surface from the bottom of the channel, H, as the length unit; the density of water, ρ_{water}, as mass unit; and the gravity constant, g. Recall that the surface tension is being neglected.

The geometry of the channel is defined by connecting several cells. In particular, since the water height is the non-dimensionalizing length unit, the non-dimensional water height is $\overline{H} = 1$, and the length of each is cell is defined to be twice $\overline{H}$, so that the interface will be initially at the middle. In total, five cells where connected so that the non-dimensional length of the channel is 10, coinciding with the value used for the linear theoretical analysis.

In order to define the interface, *Gerris* defines the density gradient along a cell following Equation 4.4 non-dimensionalized, and by means of a variable *Tracer*, which can be initialized with the shape of a given function, in this case the initial condition. The viscosity is defined in the same way. Note that, even if in the theoretical analysis it has been said that the viscosity can be neglected, here we need to define it explicitly in the code for reasons that will become clear in what follows.

Boundary conditions have to be defined for each cell at a boundary of the channel. Since the top of all cells together represents the upper boundary of the channel, for all of them the condition *BoundaryOutflow* was imposed, stating that the flow is free to leave

through this surface, and also that there is no pressure gradient along it. For the bottom of the channel, the non-penetration boundary condition is set by default for all cells. Finally, regarding the right and left boundaries of the channel, an important point is to be noted: since **the domain is periodic**, the right-most cell was connected to the left-most cell, in such a way that the channel is in itself an infinite loop in which the flow that exits through one end is exactly the one that is going to renter in the channel through the other end, yielding indeed a periodic domain. The numerical domain was defined in such a way in order to have a complete numerical simulation as similar as possible to the theoretical one, for which the domain is necessarily periodic since the analysis is done in the Fourier space, as explained in the previous Chapter 3, Section 3.6.

The following Figure 4.2 provides a schematic representation of the described numerical domain.

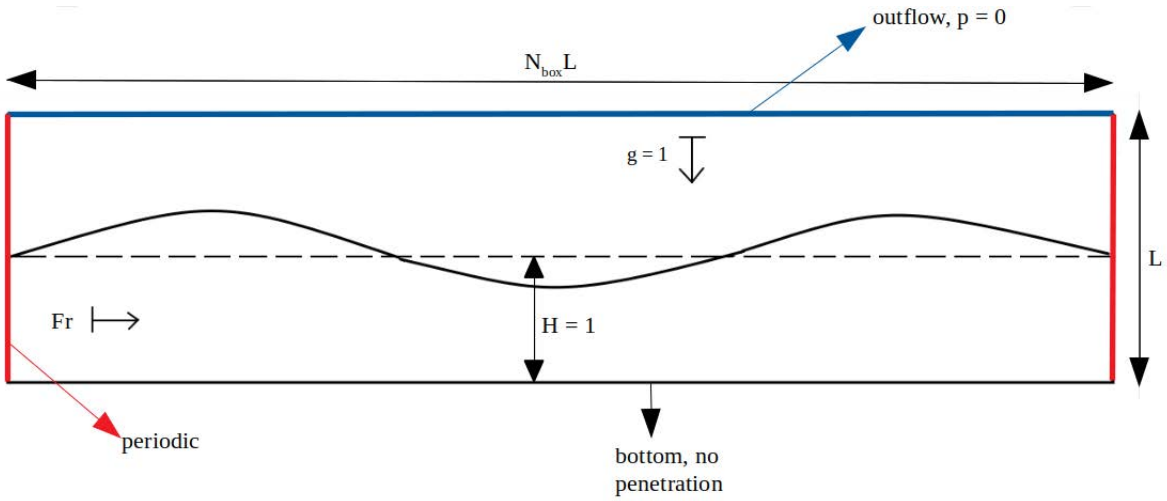

Fig. 4.2. Simulation set-up sketch.

As a final remark, *Gerris* asks the user to define the minimum and maximum levels of refinement of the adaptive mesh. The level of refinement greatly affects the accuracy of the results obtained from the simulation, since the greater the size of the cells, the greater the numerical viscosity associated to them. In this way, having an upper refinement limit not sufficiently high could lead to inaccurate results due to excessive dissipation coming from this numerical viscosity. On the other hand, increasing the level of refinement increases the computational time. In order to deal with both these situations, two measures were applied. The first one was to define explicitly the values of the viscosity for the air and

the water as it has been mentioned above. The reason to do this is that, in this way, the solver will not introduce a numerical viscosity but it will use the one provided by the user, which allows us to control the level of dissipation instead of leaving this issue a choice for the solver. The viscosity was introduced in terms of the Reynolds numbers of both fluids, which were obtained from the non-dimensionalization of the Navier-Stokes equations as:

$$Re_w = \frac{\rho_w \, g^{1/2} \, H^{3/2}}{\mu_w} \tag{4.7}$$

$$Re_a = \frac{\rho_a \, g^{1/2} \, H^{3/2}}{\mu_a} \tag{4.8}$$

in terms of the fluids' properties and the initial water height, H. A value for H of 0.225 meters was chosen following the values taken in experiments performed and found in the literature, as it was already mentioned above. Note that expressing the Reynolds number in terms of the initial water height instead of the mean current velocity is useful since it allows to fix the values for the Reynolds numbers of water and air for all those simulations in which the initial water height is the same, but with different values of the Froude number, as it is the case here. The values of the Reynolds numbers retrieved by introducing the corresponding parameter's values in Equations 4.7 and 4.8 are Re_w = 293434 and Re_a = 22720.

The second strategy has to do with the refinement method. The procedure followed consisted in defining three different levels: one for the interface between the two fluids (fixed), and then a minimum and a maximum one, used to refine the flow field according to the value of the strain rate at each cell, at each time step. The logic behind this is that we always want the maximum resolution possible for the interface, as it is there where we see the shape of the perturbation propagating. However, for the rest of the flow field, we are interested in having a higher resolution at those points in which the flow variables are changing significantly with respect to a previous step. The strain rate is the most appropriate variable to detect these changes since it indicates where there is a relative velocity between the fluid particles. In fact, the strain rate is defined as the addition of the change of the horizontal velocity in the vertical direction and the change of the vertical

velocity in the horizontal direction, i.e,

$$e_{xz} = e_{zx} = \frac{1}{2}\left(\frac{\partial u}{\partial z} + \frac{\partial w}{\partial x}\right) \tag{4.9}$$

The vorticity also provides information about the variation of the velocity field, however, for a potential flow the viscosity is zero and for this reason, the strain rate was selected instead. Actually, the variable taken for the definition of the refinement equation is not exactly the strain rate. Instead, both components in Equation 4.9 were squared in the code in order to avoid the situation in which the value of these derivatives at a given point is similar but with opposite signs, and therefore, their addition would give a small value which would result in that particular cell not being refined when there might actually be important changes in the velocity field at it. By rising both components to the second power, we make sure both of them are positive and, therefore, they cannot cancel each other out.

The actual refinement equations used are given by Figure 4.3.

```
AdaptFunction { istep = 1 } { minlevel = INILEVEL maxlevel = INTERFACELEVEL cmax = 0 } (T_mesh > 0 && T_mesh < 1)
AdaptFunction { istep = 1 } { minlevel = INILEVEL maxlevel = MAXLEVEL cmax = 1e-3 } { return T*(dy("U")*dy("U") + dx("V")*dx("V")); }
```

Fig. 4.3. Refinement equations.

Where T_{mesh} represents the variable $Tracer$ filtered, and INILEVEL, MAXLEVEL and INTERFACELEVEL are the minimum, maximum and interface refinement levels, respectively. It can be seen in the second equation of Figure 4.3 that the "strain rate" is multiplied by the $Tracer$ in order to distinguish between the air ($T = 0$) and the water ($T = 1$).

This explained refinement criteria provides efficiency in terms of computational resources, since it allows to avoid refining the entire flow field at the maximum level in order to obtain enough accuracy for the representation of the results. In this simulation the lower and upper limits of 3 and 7, respectively, were found to be a compromise between the computational time and the accuracy of the results for the flow field, while the level of refinement at the interface was set to 8.

Figure 4.4 shows the adaptive mesh zoomed in order to appreciate the refinement levels that have been described. The colors are mapped to the different values of the hori-

zontal velocity, going gradually from the minimum at the darkest blue up to the maximum at the red regions.

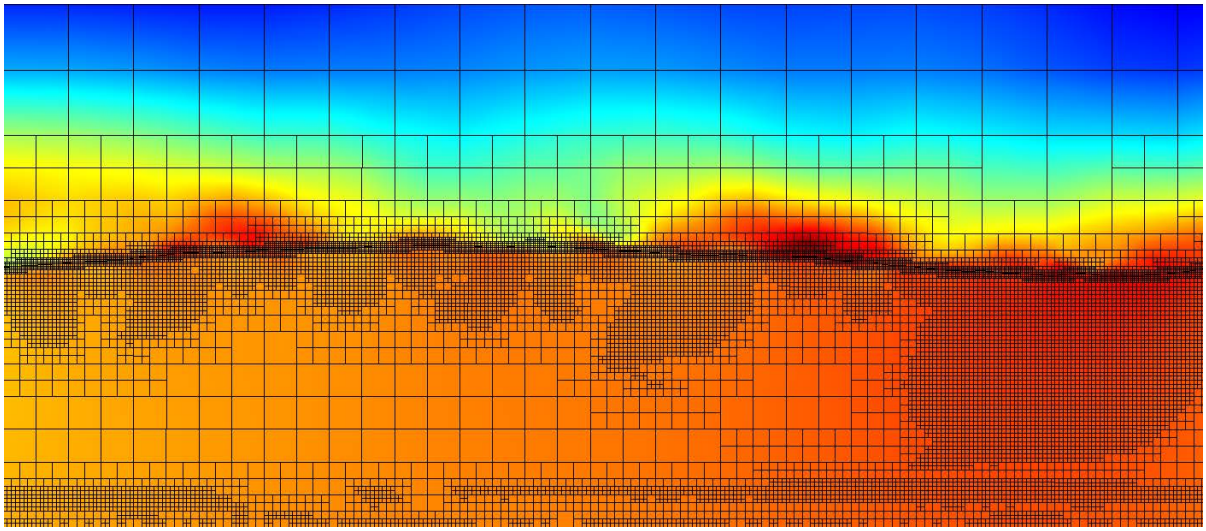

Fig. 4.4. Adaptive mesh.

4.3. Introducing an obstacle at the bottom

In order to define the domain for the channel with the bottom topography, an obstacle was introduced as a solid surface at the bottom following the shape given by Equation 3.93, in order to reach critical conditions at the throat when setting the appropriate Froude number at the beginning of the channel (we recall this was $Fr = 0.3655$). *Gerris* allows to define solids within the simulation domain by means of the command *GfsSolid*. Including a solid necessarily implies defining the level of refinement that will be applied on its surface by means of the command *GfsRefineSolid*. In this case, the level of refinement set for the bottom was 7 (MAXLEVEL).

The initial condition was redefined for this simulation. In this case, the shape followed by the perturbation on the free surface is that given by Equation 4.10, where $W = 4$, $\overline{x}_c = 14$ and f_c is the central frequency of the wave packet. Note that this wave has an amplitude too big to be in the linear regime, but this is not a concern in this case since for this simulation we are not restricted to stay within the range of the linear theory (recall that the point of the linear analysis was just to verify the validity of the numerical simulations,

as we shall show in the next chapter).

$$\eta_0(\overline{x}) = 1 + 5\,\epsilon\, e^{-\frac{(\overline{x}-\overline{x}_c)^2}{w^2}}\ \sin\left(2\pi f_c\ (\overline{x} - \overline{x}_c)\right) \tag{4.10}$$

The initial condition and its dispersion relation (zoomed) are represented in Figures 4.5 and 4.6, respectively.

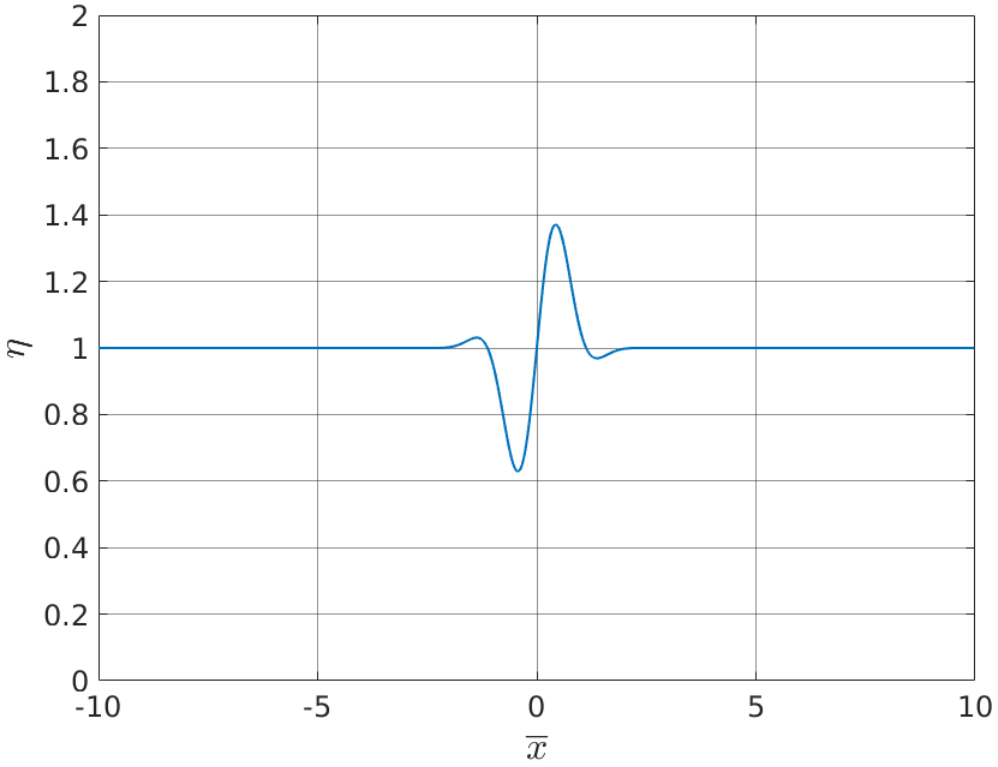

Fig. 4.5. Initial condition.

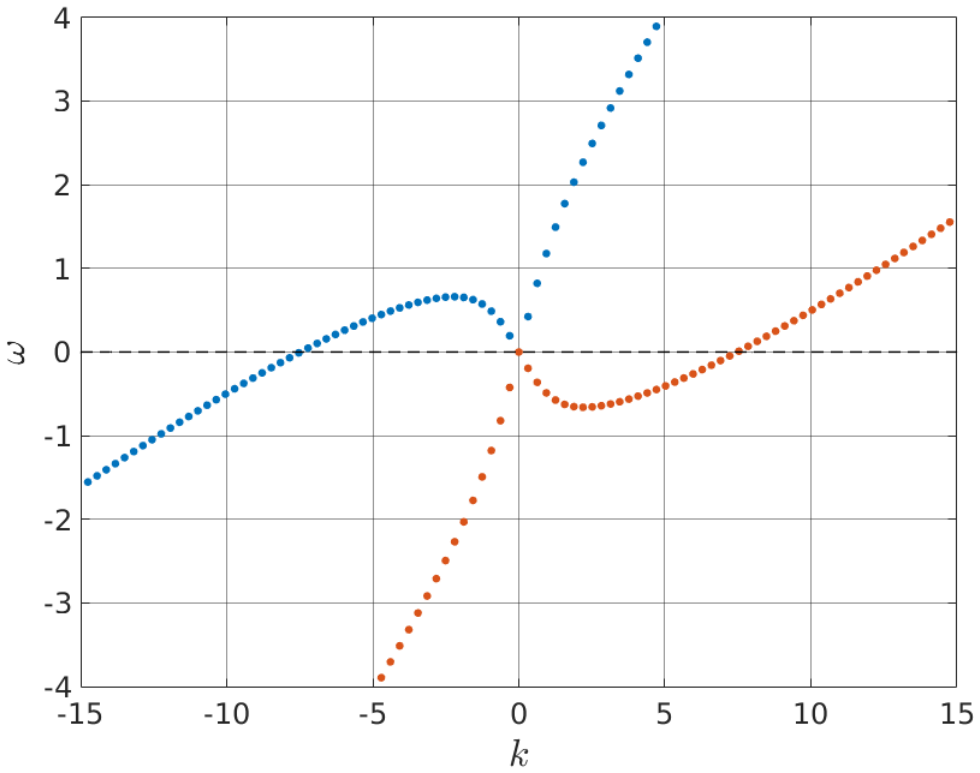

Fig. 4.6. Dispersion relation.

The Gaussian has been broadened in order to have a wave packet defined by more frequencies in the Fourier domain. Introducing a sine displaces the center of the wave packet along the frequency axis when performing the Fourier transform. Given Figure 4.6, the closest a given wavenumber is to the local minimum (or local maximum) of the curve, the higher the relation between ω and k at that frequency. If f_c is chosen to be 0.1, the Fourier transform of the initial condition yields Figure 4.7. As it can be seen, the wavenumber of the central frequency is, approximately, $k = 3$. Going back to Figure 4.6, the minimum of the curve is at $k \sim 3$. Therefore, for $f_c = 0.1$, the fastest possible wave of the packet is simulated. This is the one of interest to us since this wave is the one with better chances of reaching the throat.

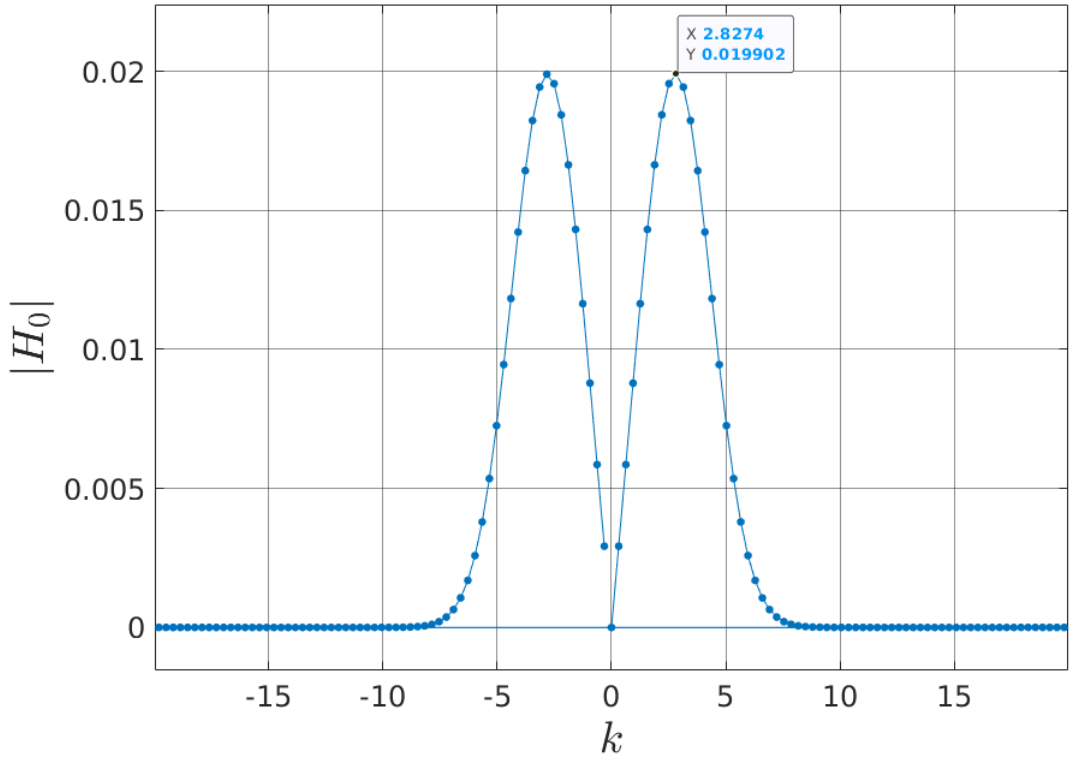

Fig. 4.7. Initial condition in the frequency domain.

Also in relation to the initial condition, note that it has been displaced to the right in the horizontal axis with respect to the previous simulation in order to allow it to propagate during the first instants without being contaminated by the effect of the bottom elevation.

Finally, the non-dimensional length of the channel is changed for this new case from 10 to 20 ($\overline{x} \in [0, 20]$), and the obstacle has its maximum height at the $\overline{x}$ coordinate located at the middle. The reason for changing the horizontal channel dimensions is to allow the initial condition to propagate up to the throat before interacting with the right branch of the perturbation, which will appear at the beginning of the channel after some time, due to the fact that the domain is periodic, as we previously explained.

The rest of the simulation features (boundary conditions, refinement method, refinement level and flow parameters) are exactly those used in the case of the channel without topography. All in all, the final simulation set-up for the case of the channel with a bottom topography can be seen in Figure 4.8.

Fig. 4.8. Initial instant for the simulation of the channel with a bottom topography.

5. RESULTS AND DISCUSSION

5.1. Homogeneous Linear Problem

We begin the analysis of the results by comparing those obtained from Airy Wave Theory and from the numerical simulation of the flow in a straight channel. Note that, since in both methods the equations have been non-dimensionalized, the results derived can be compared straightway.

First of all, the initial condition defined for the theoretical analysis and the one implemented in the numerical simulation are compared in the following Figure 5.1, in order to verify the starting points of both methods.

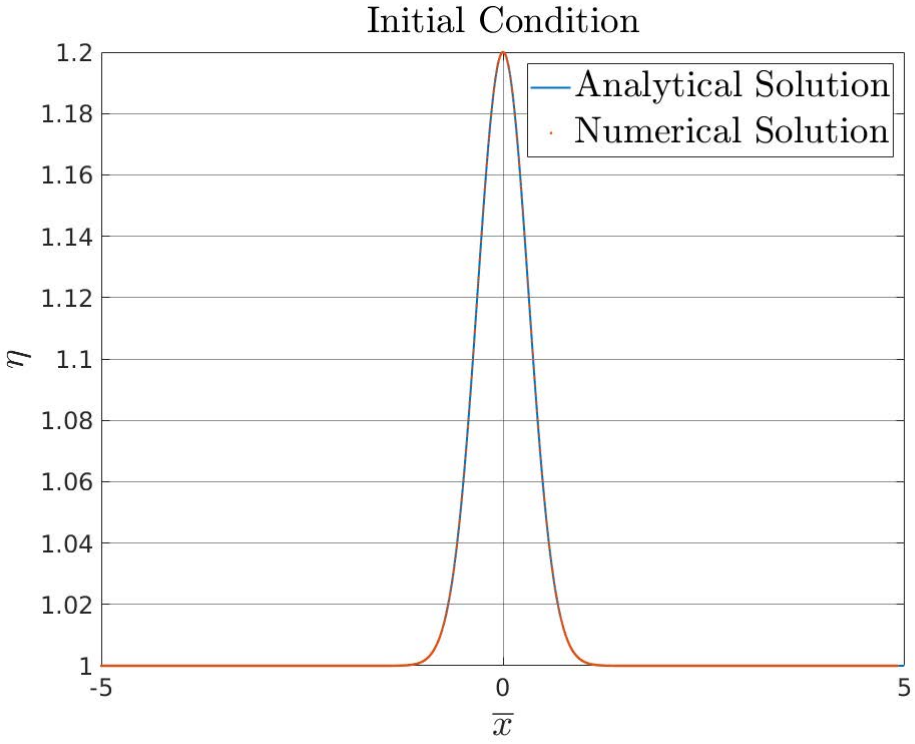

Fig. 5.1. Initial condition: $1 + 2\,\epsilon\, e^{\bar{x}^2/4}$.

As it can be seen in the figure above, the shape of the initial condition for both methods coincides.

The theoretical and the numerical results have been obtained for different Froude numbers, in particular, $Fr = 0$, 0.1, 0.5 and 1, so as to cover the limiting situation in which

there is no mean current in the channel, a case for which the mean current is so strong that no wave can propagate upstream, and two intermediate cases. Let us begin with the simplest case, the one with $Fr = 0$, i.e, with no mean current flowing in the channel.

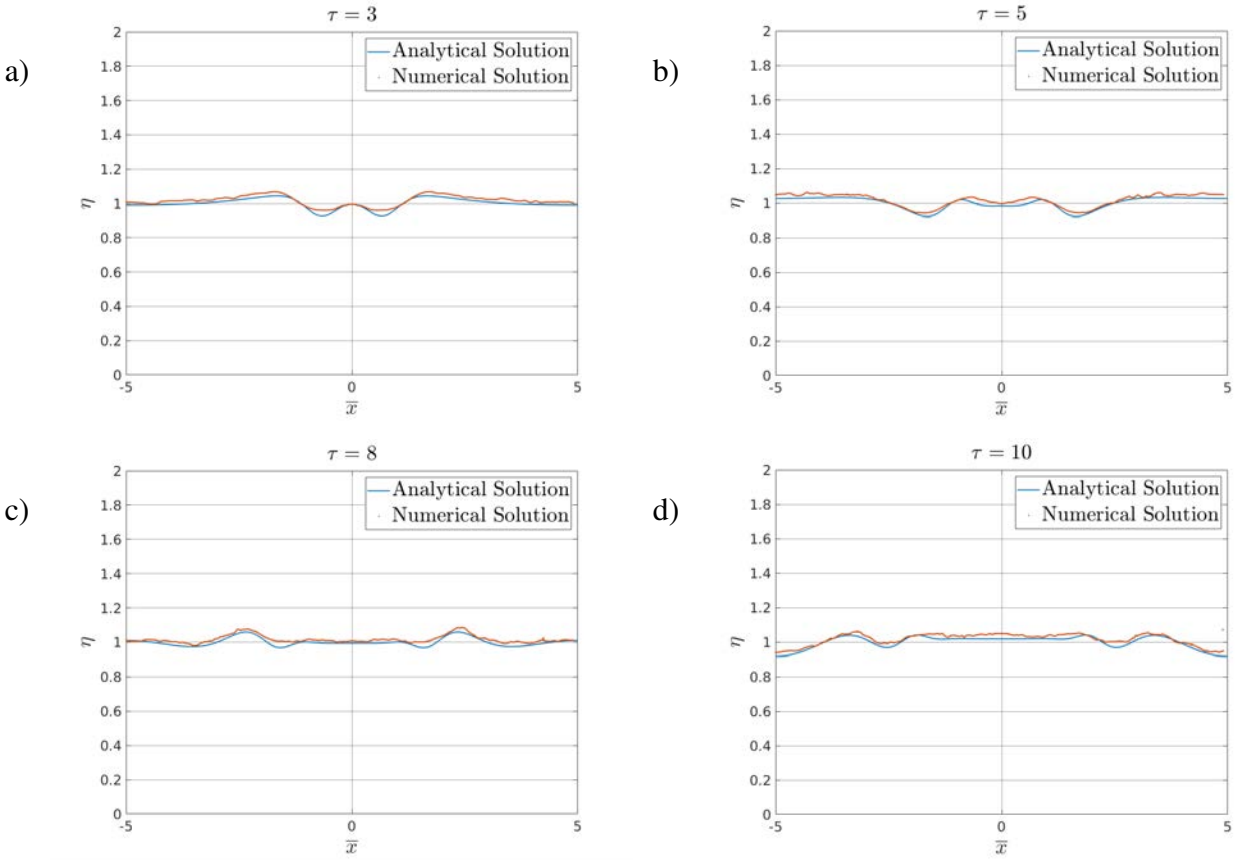

Fig. 5.2. Time evolution of the intial condition for $Fr = 0$.

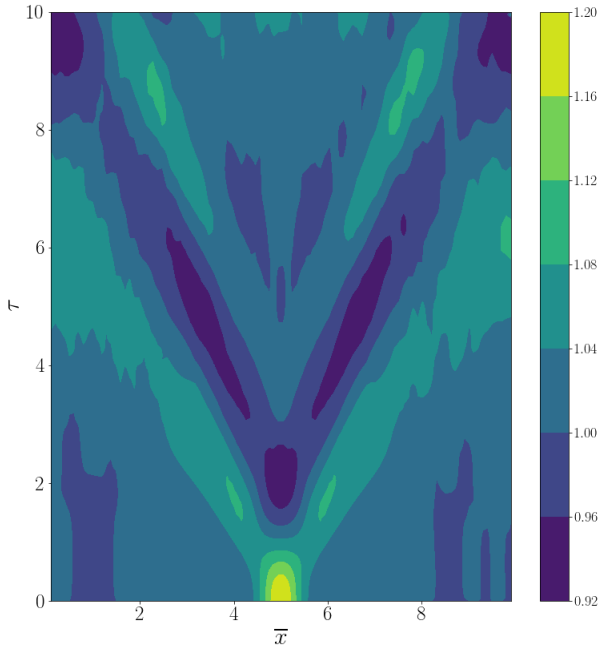

Fig. 5.3. Kymograph for $Fr = 0$.

As it can be seen in Figure 5.2, the time evolution of the initial condition given by the numerical simulation matches the one given by the analytical solution. Nevertheless, there are some differences between the two curves. One of the reasons behind this lies in the assumptions made during the theoretical analysis. Recall that the viscosity of both fluids was completely neglected during the analytical approach, while it was included in the code for the numerical simulation. The viscous effects on the flow lead to a slightly different curve at each time step. Moreover, the refinement of the mesh plays a key role as well in the accuracy of the numerical results, as explained in Chapter 4, and therefore, it is also responsible for the difference between the curves.

In Figure 5.3, the kymograph for $Fr = 0$ is given in order to appreciate the evolution of the amplitude of the wave with the time. Amplitude values are mapped to the color given by the color bar on the left.

This situation in Figure 5.2 is very similar for the different values of the Froude number mentioned above:

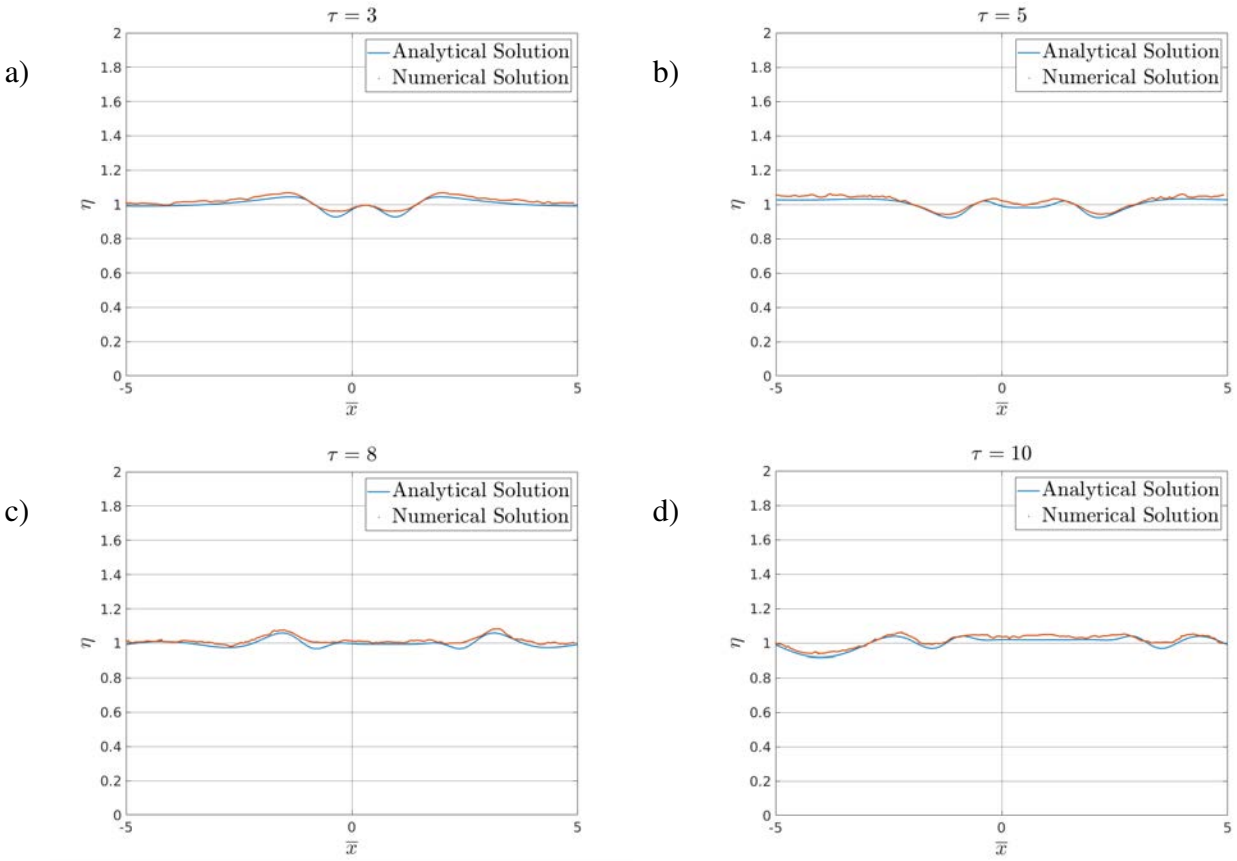

Fig. 5.4. Time evolution of the initial condition for $Fr = 0.1$.

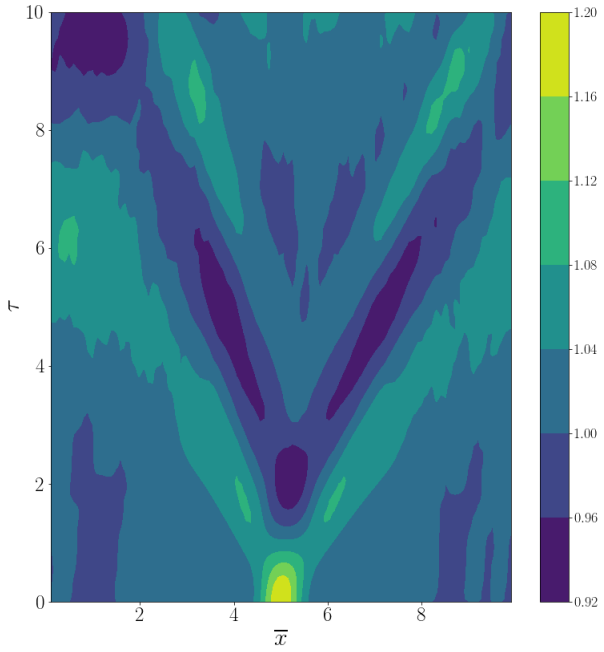

Fig. 5.5. Kymograph for $Fr = 0.1$.

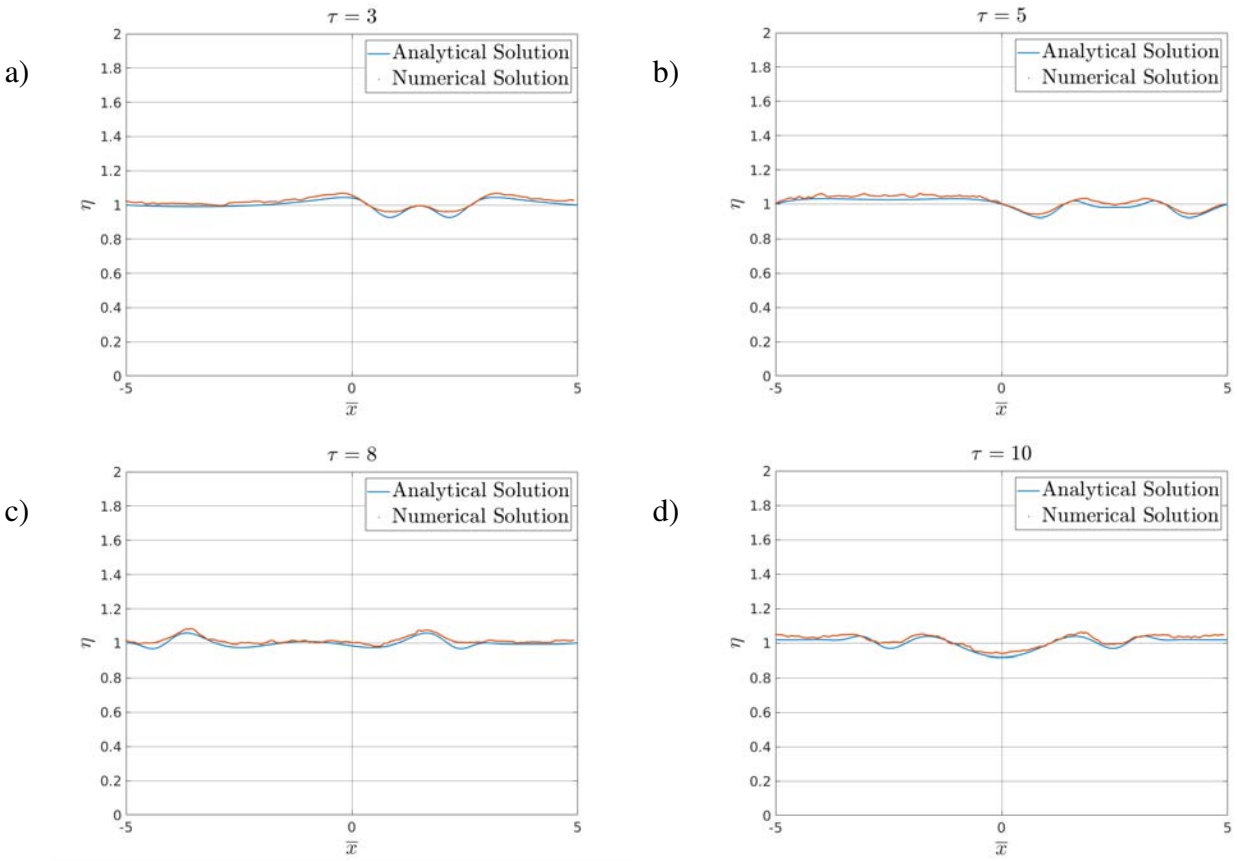

Fig. 5.6. Time evolution of the initial condition for $Fr = 0.5$.

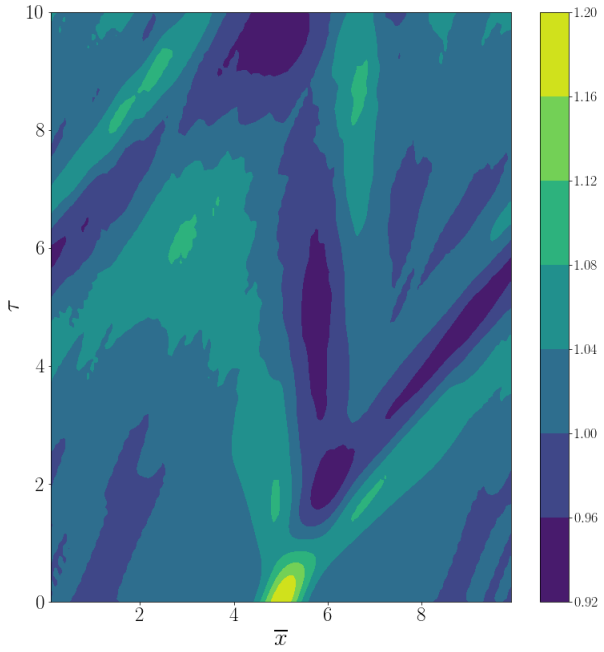

Fig. 5.7. Kymograph for $Fr = 0.5$.

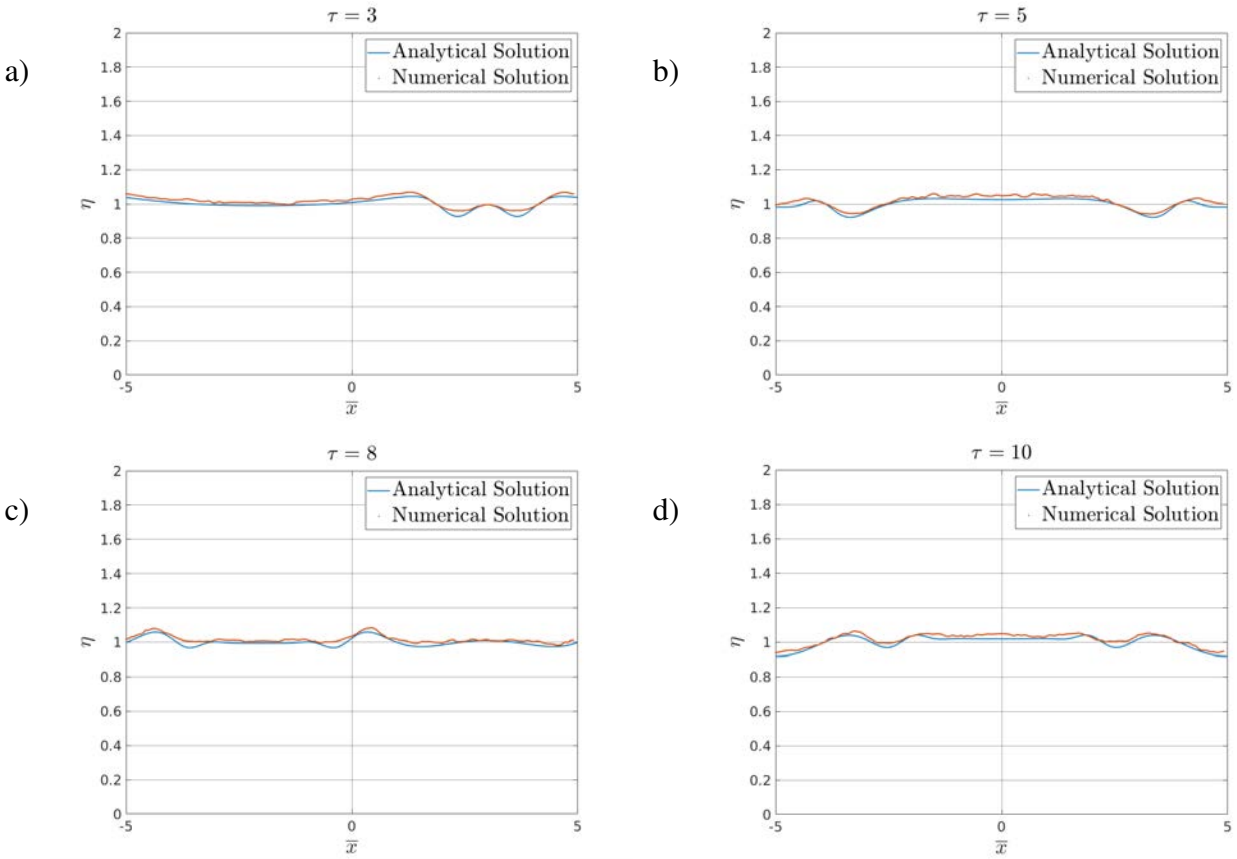

Fig. 5.8. Time evolution of the initial condition for $Fr = 1$.

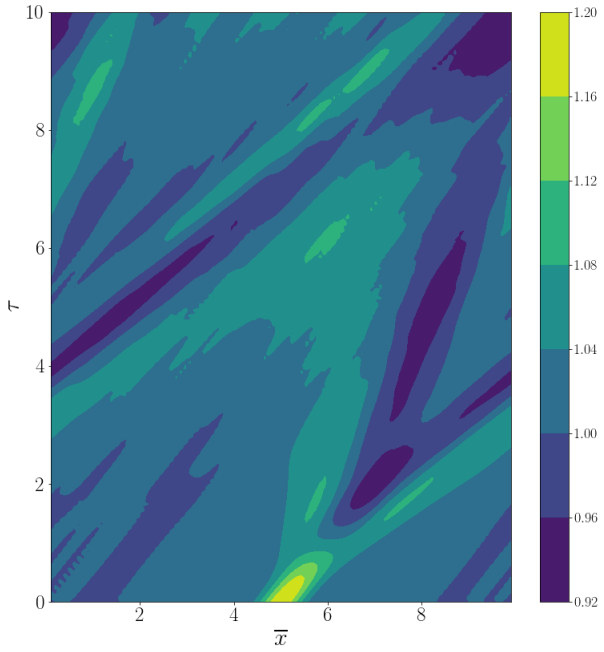

Fig. 5.9. Kymograph for $Fr = 1$.

It is interesting to compare the different graphs above and notice the effect of the Froude number on the flow. For $Fr = 0$, it can be seen that the perturbation propagates symmetrically to both sides of the channel. However, as the Froude number increases, the waves are more strongly dragged by the mean current as it is clearly represented by Figures 5.5, 5.7 and 5.9, in that order. These plots show in a very visual way the behaviour that was explained in Section 3.5.1. Such conclusion may also be extracted from Figures 5.2, 5.4, 5.6 and 5.8. Take for example the instant for $\tau = 3$. For increasing values of Fr, the wave that wants to propagate to the left finds more and more opposition from the mean current.

Finally, given the correlation between the linear theoretical results and the numerical ones shown in graphs above, it may be concluded that the numerical simulations as implemented are a valid tool to study the evolution of some initial condition in time. The next step is to use such computational methodology to study the theoretical rebound of a shallow water wave in a unitary Froude frontier, as we introduced earlier.

5.2. The limits of the Linear Theory

Before moving on to the results obtained for the flow in the channel with variable depth, it is interesting to comment on the limits of the linear theory. Recall that such theory assumes waves of small amplitude. When the amplitude of the initial condition starts to increase, the theoretical results start to diverge more and more from the numerical ones, as it is shown in Figure 5.11, for an example of an initial condition with a big amplitude (Figure 5.10), in a channel with no mean current ($Fr = 0$). Given that it has been verified that the numerical simulation is a consistent tool to analyze the evolution of the fluid, the fact that the numerical results do not match the theoretical ones when increasing the amplitude of the initial condition, means that Airy Wave Theory is no longer a valid approach to describe the evolution of the flow. Instead, higher order terms need to be considered in the analytical solution. The computation of the actual value at which the amplitude of the initial condition goes out of the linear regime is out of the scope of this report.

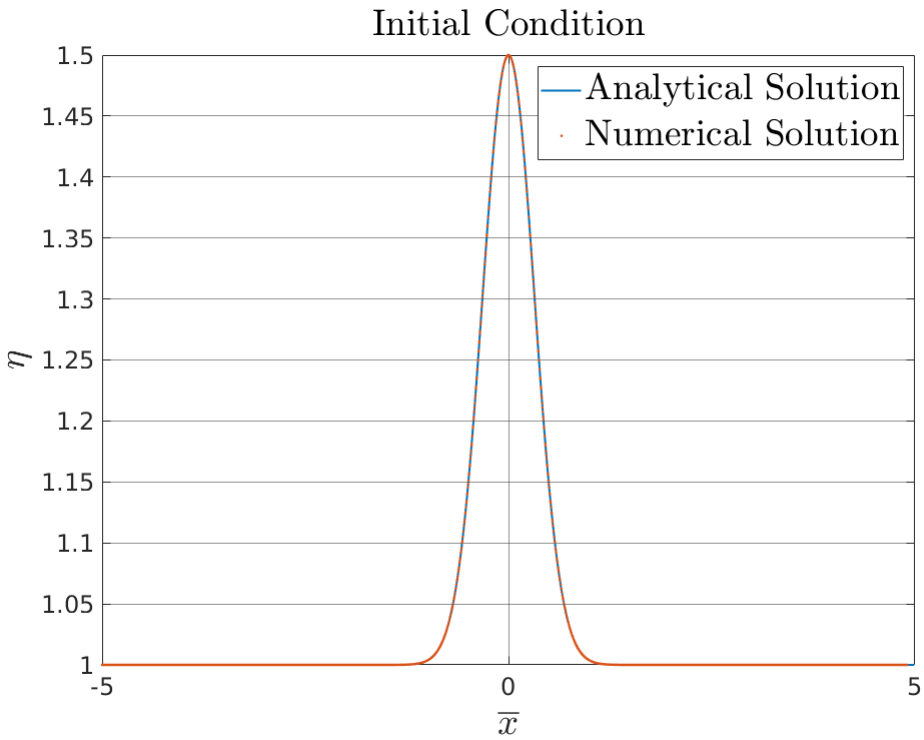

Fig. 5.10. Initial condition: $1 + 0.5\, e^{\bar{x}^2/4}$.

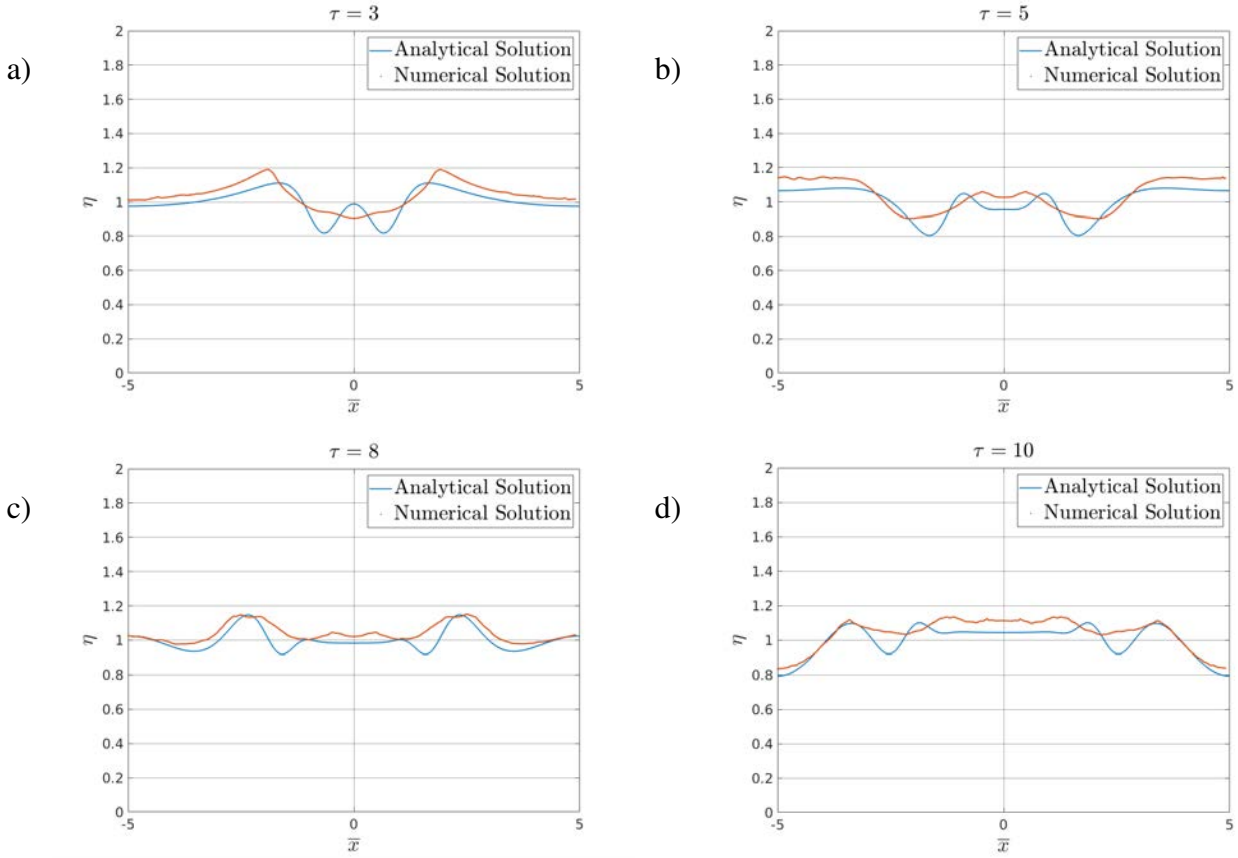

Fig. 5.11. Time evolution of the initial condition of the form $1+0.5\,e^{\bar{x}^2/4}$ in a channel with $Fr = 0$.

5.3. The channel with a bottom topography

As it was introduced above, the main objective of the linear analysis and the corresponding numerical simulations, was to verify that the latter provide us with a good tool to study more complex problems for which we do not have analytical solutions. Once the validity of the numerical approach has been proved in the previous section, the results obtained when the bottom topography is introduced are discussed in what follows. Recall that the objective of such simulations is to verify whether we can observe how the initial condition given by Equation 4.10 arrives to throat, is blocked there, and gives place to two deep-water waves.

Figure 5.12 represents the time evolution of the free surface at two different fixed $\overline{x}$ stations. Figure 5.13 illustrates with a color line mapped to the amplitude of the waves, the evolution of the simulation. Finally, Figure 5.13 provides different time instants to clearly visualize the behaviour of the fluid as the initial perturbation propagates.

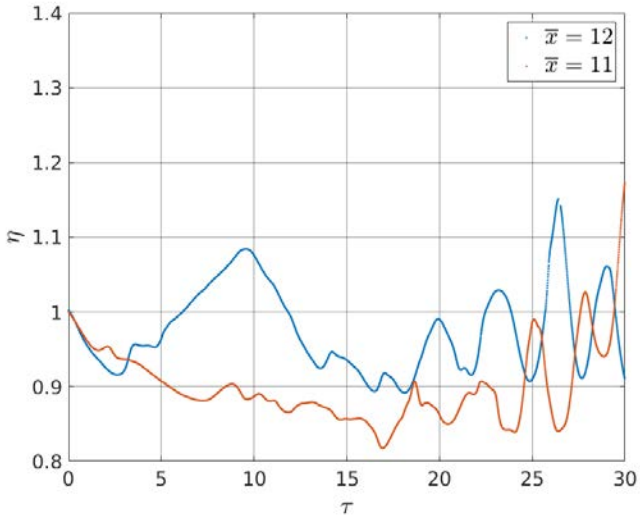

Fig. 5.12. Time evolution of the free surface at $\overline{x} = 11$ and $\overline{x} = 12$.

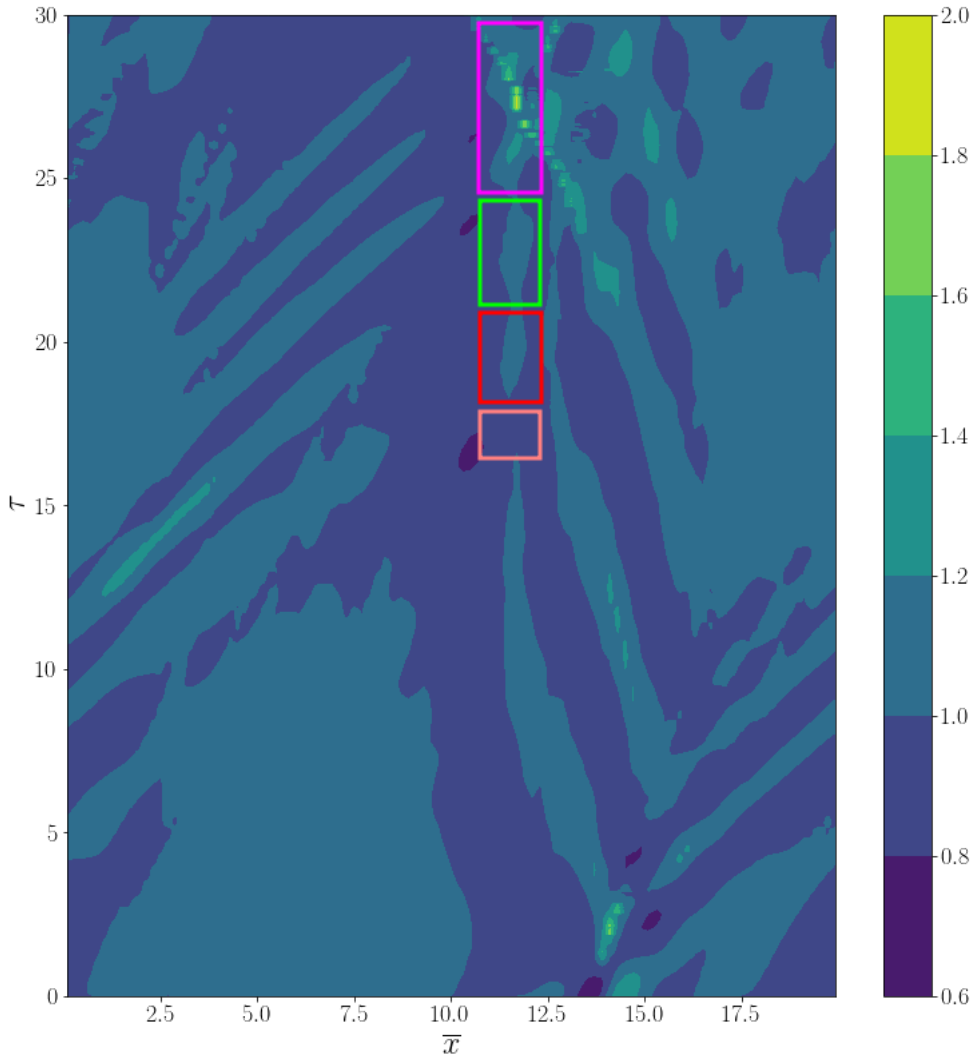

Fig. 5.13. Time evolution of the simulation given by the color-mapped amplitude of the waves.

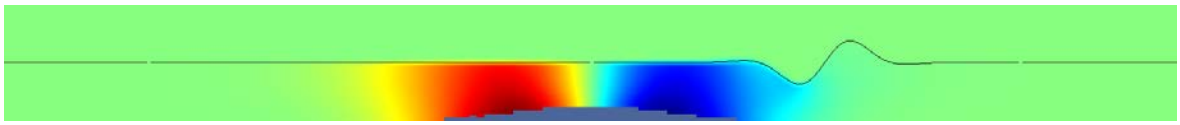

(a)

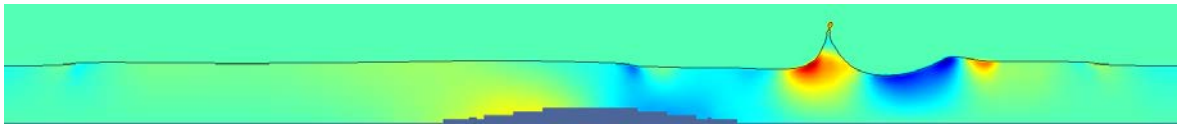

(b)

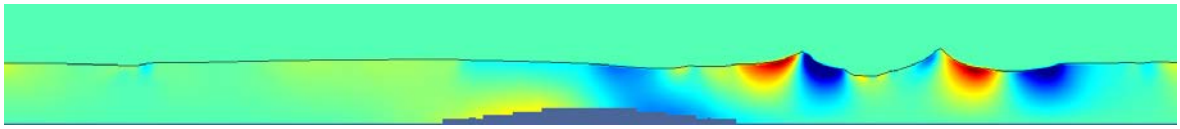

(c)

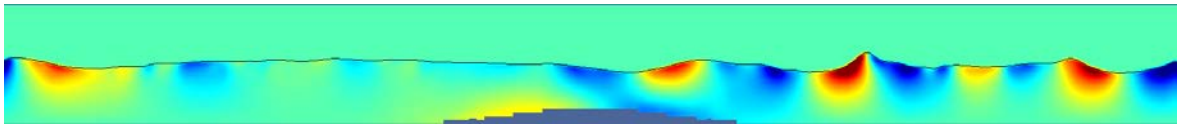

(d)

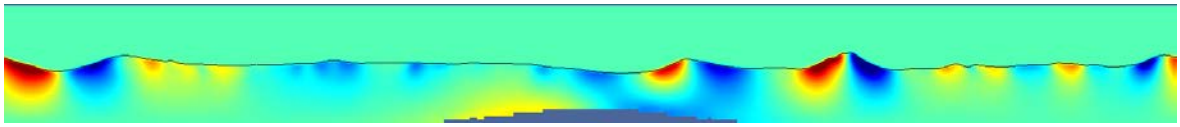

(e)

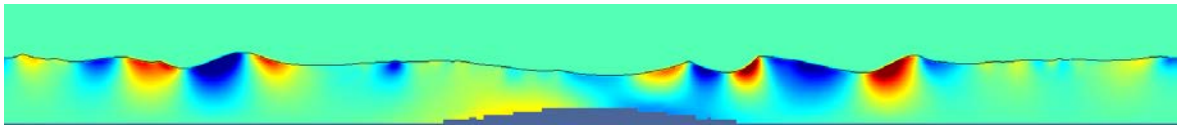

(f)

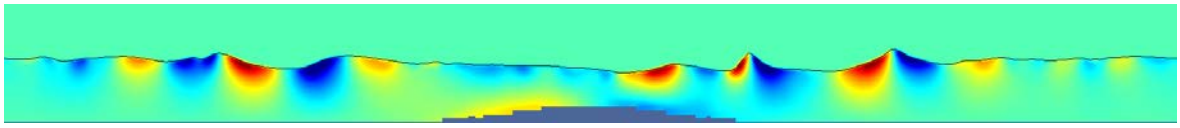

(g)

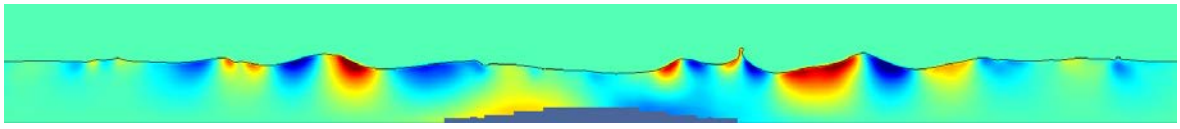

(h)

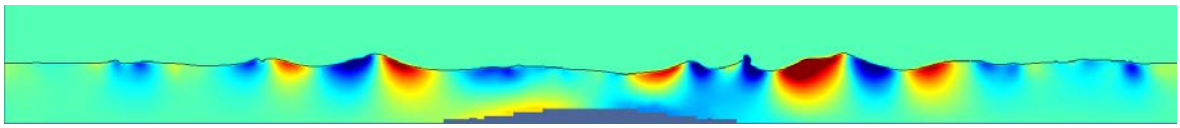

(i)

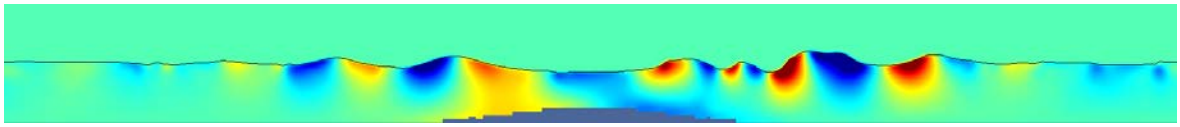

(j)

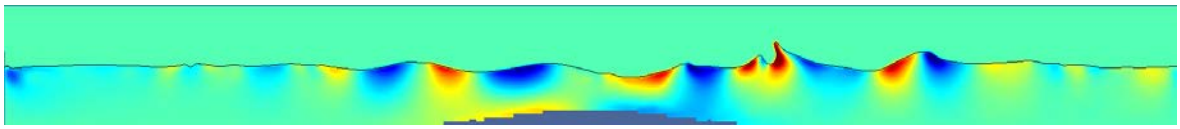

(k)

Fig. 5.13. (a) $\tau = 0.00$, (b) $\tau = 2.00$, (c) $\tau = 4.30$, (d) $\tau = 9.00$, (e) $\tau = 11.00$, (f) $\tau = 16.00$, (g) $\tau = 18.00$, (h) $\tau = 20.00$, (i) $\tau = 21.00$, (j) $\tau = 22.50$, (k) $\tau = 24.00$. Red for positive vertical velocity, blue for negative vertical velocity.

Rely on the figures above to support the following explanation. The initial perturbation is a wave with big amplitude and it propagates both to the left and to the right. This can be most clearly seen in Figure 5.13, where the initial perturbation is given by the initial zone in yellow, and the subsequent waves it generates in both directions can be seen in the different scales of blue. The lighter the blue, the higher the amplitude. As the initial propagation advances towards the left of the channel (branch which is of interest to us, since it is the one approaching the throat), its amplitude is attenuated. This can be seen especially in Figure 5.12, where at $\overline{x} = 12$ the wave is still strong, but already at $\overline{x} = 11$, it has been quite attenuated due to the effect of the incoming current. Around $\tau = 9$ ((d) in Figure 5.13), the left side of the perturbation reaches the throat and it is blocked. From that instant on, the following incoming waves that reach the throat also start to die there, until around $\tau = 16$ (f), they appear to die completely. This is also represented in Figure 5.13 by the region inside the pink box, and it may also be observed in Figure 5.12 that the curve for $\overline{x} = 11$ reaches a particularly low minimum. From this point, the free surface of water starts to rise again and approximately at $\tau = 18$, it can be clearly seen that a new wave appears propagating in the opposite direction, this is, to the right. This may be more clearly seen in Figure 5.13 (g) where the positive vertical velocity has increased

significantly with respect to the previous instant depicted, in which the incoming wave had already died. This first wave is also shown in Figure 5.13 as the region inside the red box. Around $\tau = 20$, such wave starts to die due to its interaction with the incoming waves that are still propagating to the left. This may be seen in Figure 5.12, where the free surface of water is seen to decrease, and also in Figure 5.13 (h), where the positive vertical velocity has decreased while the negative one has increased with respect to the previous step. Later on, at the instant $\tau = 21$, the free surface rises again and, similarly, the positive vertical velocity starts to increase (Figure 5.13 (i)). This second wave is observed to die around $\tau = 22.5$ (j), for the same reasons as the first one. It could be argued that these are the two rebounded waves we were expecting to find, however, the results are not conclusive because there also exits the possibility that the two peaks shown in Figure 5.12 at $\tau \sim 18$ and $\tau \sim 21$ are due to the initial wave, which is back after going all the way around the numerical domain. In this case, the initial wave approaching from the left would have been attenuated before reaching the throat, and this is why it is not depicted in lighter blue (big amplitude) in Figure 5.13. Finally, approximately at $\tau = 24$, the right branch of the initial perturbation which appeared at the left end of the channel due to the periodicity of the domain, effectively reaches the throat, destroying the critical region and any possibility of observing the theoretical deep-water waves. This is represented by the zone in the purple box in Figure 5.13, and it may also be appreciated by the significant increase of the free surface after this instant in Figure 5.12.

The results shown seem to indicate that the incoming initial perturbation is indeed blocked but they do not allow us to guarantee the appearance of the two deep-water waves. In order to reach solid conclusions, further simulations considering the attenuation of the right branch of the initial condition, capillarity, a higher refinement of the throat region and a more thorough post-processing should be conducted. This process would be quite time-consuming and for this reason, it is out of the scope of this report. As it was introduced at the beginning, the goal of this project was to reproduce with a numerical simulation the experiments performed by S. Weinfurtner et al. in [1] in order to develop a valid numerical tool for the study of the propagation of gravity waves in water. The results obtained show the promising use of the tool developed and set the basis to continue with further studies on the topic.

5.4. Quantum Analogies

A thorough explanation of concepts of Quantum Mechanics is out of the scope of this report, however, given the fundamental motivation of this project, it is interesting to end the discussion of the results by giving some notions about the applications of the tool that has been developed in the study of Quantum Mechanics problems.

As introduced at the beginning of this report, an open channel flow may be used as an analogy to the event horizon of a white hole. The reason is that the mathematical relation between the amplitudes of the two short waves appearing in the channel is the same as that between the waves associated to the two subatomic particles resulting from a pair creation [1].

A black hole is a region of spacetime with a gravitational acceleration so big that not even electromagnetic radiation can escape from it. The boundary of such region is called the *event horizon* of the black hole. In contrast, a white hole is an **hypothetical region** of spacetime from which matter and radiation can escape, but into which nothing can enter. In this sense, a white hole may be understood as the reverse of a black hole. In 1974, Stephen Hawking suggested that in the event horizon of a black hole, photons are constantly being created and annihilated. Given the strong gravitational attraction at such region, it may occur that after a pair creation process and before the two particles annihilate each other back into a photon, one of the two gets absorbed into the black hole, while the other one escapes the gravitational pull and it leaves as if *emitted* by the black hole. This process is called *Hawking radiation* and it explains the fact that the mass of a black hole decreases over time if it is not increased by other means (*black hole evaporation*)[30].

Since the black hole emits radiation, it may arrive to a thermal equilibrium state. Such state is time-reversal-invariant, therefore, the time-reverse of a black hole in thermal equilibrium is also a black hole in thermal equilibrium. This conclusion led Stephen

[1] In Quantum Mechanics, pair creation is the process by means of which a subatomic particle and its antiparticle (a particle with the same mass as the first one but opposite electrical charge) are created from a neutral boson. A photon (a particle of light) with enough energy can be decomposed into an electron and a positron (the antiparticle of the electron). Similarly, an electron and a positron that find each other in space and time *annihilate* one another to give a photon.

Hawking to state that white holes and black holes are actually the same object, given the definition of a white hole provided before. In turn, this implies that the Hawking radiation of a black hole is the white-hole emission. [31]

Up to this point it may appear that black and white holes are a field of study very distant from the propagation of gravity waves in water. However, note that the event horizon of a white hole is analogous to the frontier of $Fr = 1$ in the channel, in the sense that it does not allow waves (light is a form of electromagnetic radiation, i.e, a wave) to penetrate into the other side. When a pair creation process takes place at the event horizon of a white hole and one of the particles gets absorbed while the other one is emitted, it turns out that the mathematical relation between the amplitude of the waves associated to such particles [2] is the same as the relation between the amplitudes of the two short waves created from the shallow-water wave in the channel [1]. In this way, the usefulness of the tool developed during this project can be appreciated, as it allows to establish an experimental analogy between the channel and a purely theoretical system such as a black hole. More importantly, detailed numerical simulations of the fluid-mechanical analogy will allow us to determine to what extent the analogy really holds. In future works, other effects can be explored with the numerical tool developed here, to name a few, how non-linearity affects the analogy, effect of surface tension, and effect of a larger viscosity.

Moreover, this tool can be used for the study of other Quantum-related phenomena. To give some other interesting examples, we may consider the electron cloud of a metal or the alpha decay of unstable atomic nuclei in a potential sink [32].

In relation to the first of them, electrons in a metal move in a region where their potential energy is approximately constant due to the properties of the metallic bond (the "*electron cloud*"). When an electron reaches the end of such region, it is pushed back inside because it does not have enough energy to pass through it and leave the metal. Recall that quantum entities can be described both by means of particles and by means of waves. Then an electron is a wave, and when it reaches the boundary of the electron cloud, it is blocked. This situation is again analogous to the blocking of the gravity wave in the throat of the channel.

[2] The wave-particle duality states that every particle or quantum entity can be described in terms of both particles and waves.

The situation is similar in the second example. Some atomic nuclei emit α particles, which are given by two protons and two neutrons bound together. The theory of α decay states that such particles are retained in the nucleus due to the action of forces similar to those keeping together the neutrons and the protons of the nucleus itself. Such forces have a very short range of action (of the order of the nuclear radius), therefore, outside the nucleus, their effect on an α particle is negligible. Imagine the situation in which an α particle is approaching the nucleus from far outside.. At the beginning, it will be repelled by the electrostatic force, since both the particle and the nucleus are positively charged (Coulomb repulsion). However, once inside the nucleus, the nuclear force will balance the electrostatic repulsion, as it may be seen in Figure 5.14. In fact, if the α particle does not have enough energy to reach the Coulomb repulsion branch of the potential, it will become trapped inside the nucleus. In definitive, the particle (the wave) will be blocked by a potential barrier, as in the case of the channel again.

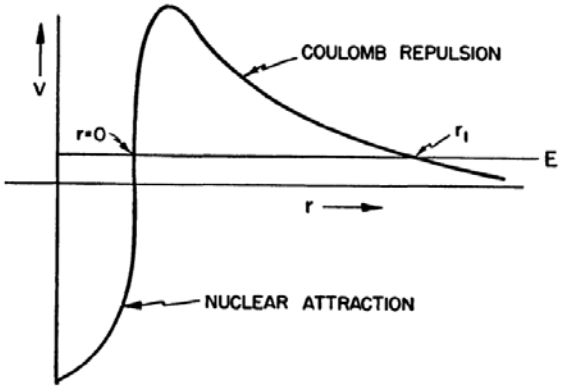

Fig. 5.14. Potential curve of an α particle as function of the distance to the center of the nucleus. [32]

6. CONCLUSIONS AND FUTURE WORK

Along this project, we have developed a computational tool that allows the study of the propagation of gravity waves in water. In order to do so, we reproduced with a numerical situation the conditions of an experimental study performed by S. Weinfurtner et al. and published in the *Physical Review Letters*, in which a shallow water wave propagating upstream in a flume is blocked when it reaches a high-velocity region of the flow, and subsequently decomposed into two deep-water waves. The key points of this work are outlined in what follows.

First of all, a theoretical analysis of the problem was performed. The starting point was a simpler version of the actual problem, in which we consider the propagation of a perturbation in a straight channel with a mean flow. An analytical expression for the evolution of the velocity potential and the height of the free surface in time can be obtained for such case by means of the Airy Wave Theory (Linear Wave Theory). We saw that even if the linear approach is useful for some purposes, such as checking the validity of the numerical tool, it only works under restrictive conditions, namely, small-amplitude waves and a constant-depth domain. Therefore, its applications are limited and in order to study the evolution of a flow in a channel with a bottom topography, Shallow Water Theory needs to be used instead.

The solution of the homogeneous linear problem was obtained and provided us with an important result: the dispersion relation. Such equation states the dependency between the frequency and the wavenumber of the waves that can exist in the channel after the initial perturbation occurs. It also shows the influence of the flume velocity on the propagation of these waves (by means of the Froude number), allowing us to determine which waves are able propagate upstream in the channel, and which other will be dragged by the mean current.

In order to study the time evolution of the waves in the channel, Fourier analysis needs to be used. The time evolution of the initial condition can be determined from the time evolution of its Fourier coefficients.

To conclude with the theoretical analysis, we saw that in order to reach the desired

conditions at the throat of the channel (critical Froude number), the geometry of the topography and the initial velocity of the mean flow need to satisfy a certain relation given by the Shallow Water Equations.

In the second part of the project, numerical simulations were performed by means of the *Gerris Flow Solver*. It was shown that *Gerris* is able to describe with high accuracy the evolution of a flow under given conditions.

Given the correlation between the linear analytical results and the numerical ones, we were able to state the validity of the numerical tool developed. This allowed us to use this tool to study the evolution of a flow in a channel with a bottom topography, with the aim of observing the rebound of a long water wave into two short waves. The results obtained from this simulation were not conclusive, which sets a starting point to continue with future studies.

Finally, it is interesting to comment on some points of the present study that could be further investigated in order to improve the validity of the computational tool developed. Some ideas are listed below:

- Study the effect of viscosity by performing simulations in which this parameter is modified.
- Redefine the refinement strategy in order to focus on the throat region and obtain a higher resolution of the flow variables there.
- Include in the simulations the term of the surface tension in order to consider the presence of capillary waves.
- Work on strategies to attenuate the waves coming from the left end of the channel, in order to find out whether those waves are actually contaminating the rebound we seem to observe.
- Perform experiments in an actual channel reproducing the conditions of the simulation to confirm if the rebound of the long water wave is observed.

BIBLIOGRAPHY

[1] S. Weinfurtner, E. W. Tedford, M. C. J. Penrice, W. G. Unruh, and G. A. Lawrence, "Measurement of stimulated hawking emission in an analogue system", *Phys. Rev. Lett.*, vol. 106, p. 021 302, 2 Jan. 2011. DOI: 10.1103/PhysRevLett.106.021302. [Online]. Available: https://link.aps.org/doi/10.1103/PhysRevLett.106.021302.

[2] *Seaborn seaplane*, https://www.seaborneairlines.com/st-thomas/seaplane/, Accessed: 2019-06-08.

[3] NASA, *Apollo 16 splashdown*, https://www.nasa.gov/image-feature/apollo-16-splashdown, Accessed: 2019-06-08.

[4] T. N. Y. Times, *Aricraft carrier*, https://www.nytimes.com/2017/04/18/world/asia/aircraft-carrier-north-korea-carl-vinson.html, Accessed: 2019-06-08.

[5] SpaceX, *Falcon 9 first stage*, https://www.spacex.com/gallery/2016-0#slide-5, Accessed: 2019-06-08.

[6] G. Rousseaux, P. Maïssa, C. Mathis, T. G. Philbin, and U. Leonhardt, "Observation of negative-frequency waves in a water tank: A classical analogue to the hawking effect?", *New Journal of Physics*, vol. 10, p. 053 015, 5 May 2008. DOI: 10.1088/1367-2630/10/5/053015. [Online]. Available: https://doi.org/10.1088%5C%2F1367-2630%5C%2F10%5C%2F5%5C%2F053015.

[7] G. Rousseaux *et al.*, "Horizon effects with surface waves on moving water", *New Journal of Physics*, vol. 12, p. 095 018, 9 Sep. 2010. DOI: 10.1088/1367-2630/12/9/095018. [Online]. Available: https://doi.org/10.1088%5C%2F1367-2630%5C%2F12%5C%2F9%5C%2F095018.

[8] Y. Goda, *Random Seas And Design Of Maritime Structures (Advanced Series On Ocean Engineering)*, 3rd. Singapore, China: World Scientific Publishing Co Pte Ltd, 2010.

[9] S. A. Hughes, *Physical Models and Laboratory Techniques in Coastal Engineering (Advanced Series On Ocean Engineering)*, 1st. Singapore, China: WORLD SCIENTIFIC, 1993.

[10] V. Singal, J. Bajaj, N. Awalgaonkar, and S. Tibdewal, "Cfd analysis of a kerosene fuel tank to reduce liquid sloshing", *Procedia Engineering*, vol. 69, pp. 1365–1371, 2014, 24th DAAAM International Symposium on Intelligent Manufacturing and Automation, 2013. DOI: https://doi.org/10.1016/j.proeng.2014.03.130. [Online]. Available: http://www.sciencedirect.com/science/article/pii/S1877705814003762.

[11] M. Hosain, U. Sand, and R. B. Fdhila, "Numerical investigation of liquid sloshing in carrier ship fuel tanks", *IFAC-PapersOnLine*, vol. 51, no. 2, pp. 583–588, 2018, 9th Vienna International Conference on Mathematical Modelling. DOI: https://doi.org/10.1016/j.ifacol.2018.03.098. [Online]. Available: http://www.sciencedirect.com/science/article/pii/S2405896318301022.

[12] (2000). Recommended practice for planning, designing and constructing fixed offshore platforms—working stress design, [Online]. Available: http://latorebondeng90245.tripod.com/api_rp2a.pdf.

[13] (1988). Lrs code for offshore platforms, [Online]. Available: https://www.lr.org/en/marine-shipping/naval/.

[14] (2005). Solas - international convention for the safety of life at sea, [Online]. Available: http://www.mar.ist.utl.pt/mventura/Projecto-Navios-I/IMO-Conventions%5C%20(copies)/SOLAS.pdf.

[15] (2009). Naval ship code, [Online]. Available: http://www.navalshipcode.org/naval-ship-code/.

[16] (), [Online]. Available: https://www.faa.gov/regulations_policies/faa_regulations/.

[17] (), [Online]. Available: https://www.easa.europa.eu/regulations.

[18] R. B. Dean and R. A. Darlymple, *Water Wave Mechanics for Engineers and Scientists*, 1st. New jersey, USA: Prentice hall, 1984.

[19] L. Landau and E. Lifshitz, *Course of Theoretical Physics, Volume 6: Fluid Mechanics*, 2nd. Oxford, UK: Elsevier, 1987.

[20] MIT, *Hydrodynamics*, https://ocw.mit.edu/courses/mechanical-engineering/2-016-hydrodynamics-13-012-fall-2005/readings/2005reading7.pdf, Accessed: 2019-06-08.

[21] R. A. Guijarro. (2019). Numerical and experimental analyses of a piston-type wavemaker in a 2d flume. Master Thesis, [Online]. Available: https://e-archivo.uc3m.es/handle/10016/16118.

[22] M. V. Torres. (2012). Verificación experimental de la analogía de la emisión estimulada de hawking con ondas gravitatorias en un canal (spanish). Bachelor Thesis, [Online]. Available: https://e-archivo.uc3m.es/handle/10016/16084#preview.

[23] P. LibreTexts, *The heisenberg uncertainty principle*, https://phys.libretexts.org/Bookshelves/University_Physics/Book%3A_University_Physics_(OpenStax)/Map%3A_University_Physics_III_-_Optics_and_Modern_Physics_(OpenStax)/7%3A_Quantum_Mechanics/7.2%3A_The_Heisenberg_Uncertainty_Principle, Accessed: 2019-06-08.

[24] B. Levich, *Theoretical Physics, Volume 1: Theory of the Electromagnetic Field, Theory of Relativity*, 1st. Oxford, UK: Elvesier, 1971.

[25] MathWorks, *Fast fourier transform animation using matlab*, https://es.mathworks.com/matlabcentral/fileexchange/53674-fast-fourier-transform-fft-animation-using-matlab, Accessed: 2019-06-08.

[26] MIT, *The shallow water equations*, http://www-eaps.mit.edu/~rap/courses/12333_notes/A2%20SWeqs.pdf, Accessed: 2019-06-15.

[27] H. Liepmann and A. Roshko, *Elements of Gasdynamics*, 1st. USA: Dover Publications, 2001.

[28] S. Popinet, "Gerris: a tree-based adaptive solver for the incompressible Euler equations in complex geometries", *Journal of Computational Physics*, vol. 190, no. 2, pp. 572–600, 2003. DOI: 10.1016/S0021-9991(03)00298-5.

[29] ——, “An accurate adaptive solver for surface-tension-driven interfacial flow”, *Journal of Computational Physics*, vol. 228, no. 2, pp. 5838–5866, 2009. DOI: 10.1016/j.jcp.2009.04.042.

[30] S. Hawking, “Black hole explosions?”, *Nature*, vol. 248, no. 5443, pp. 30–31, 1974. DOI: 10.1038/248030a0.

[31] S. W. Hawking, “Black holes and thermodynamics”, *Phys. Rev. D*, vol. 13, pp. 191–197, 2 Jan. 1976. DOI: 10.1103/PhysRevD.13.191. [Online]. Available: https://link.aps.org/doi/10.1103/PhysRevD.13.191.

[32] D. Bohm, *Quantum Theory*, 1st. New York, USA: Dover Publications, 1989.